Impacts of Summer Cyclones on Arctic Sea Ice

Claire Mundi

A Thesis submitted in partial fulfillment of

the requirements for the degree of

Master of Science

(Atmospheric and Oceanic Sciences)

at the

UNIVERSITY OF WISCONSIN-MADISON

August 2022

Abstract

Impacts of Summer Cyclones on Arctic Sea Ice

by Claire Mundi

As Arctic sea ice approaches its seasonal minimum in mid-September, the sea ice (particularly around the ice edge) is left thin and vulnerable to breakup by mechanical, thermodynamic, and radiative forces, which are potentially enhanced by the presence of late-summer cyclones. Previous studies remain inconclusive as to the exact ice response caused by extreme summer cyclones, with some studies citing enhanced loss and others claiming the storms help preserve ice during the summer decline. Two distinct case studies are examined using satellite observations and reanalyses to illustrate each of these responses. The first case study shows a storm with dominant northerly winds and a warming trend of sea surface temperature within the marginal ice zone, corresponding with a more rapid decrease in sea ice area during the cyclone lifetime. The second case study demonstrates an instance where the sea ice area within the marginal ice zone is increasing relative to the background summer melt, likely due to the cyclone's dominant southerly winds advecting the sea ice northwards into regions of lower SST. Using the relationships defined in these two processes, four categories were defined based on the storms' dominant wind direction (northerly or southerly) and sea surface temperature trends (warming or cooling) to demonstrate the impacts of a census of 21 storms from August and September 2007-2010. A composite analysis was then performed on each of

these categories to summarize the effects of each of these storm types on the observed sea

ice trends.

Acknowledgements

First and foremost, I would like to thank my advisor Tristan L'Ecuyer for all of his advice and support over the past two years. I would also like to thank Jon Martin for all his helpful discussions on this topic, as well as Till Wagner for his feedback on this thesis and suggestions for future work.

Additionally, I would like to offer my appreciation to everyone in our research group, as well as all my fellow graduate students in the department for all their friendly conversations and research help. A special thanks to Ian Beckley for always being open to sharing ideas about this project, as well as for the contributions of Figures 3.1 and 3.10 (and the discussions therein).

The entire AOS community of students, faculty, and staff has made starting graduate school during a pandemic much better than expected.

I would also like to thank my friends and mentors from Skidmore who helped me learn to love research and for their encouragement in starting this journey.

Lastly, and most importantly, I'm appreciative of the constant support from my mom, dad, and brother. I would not have made it this far without your never-ending enthusiasm for my education and career.

Contents

List of Figures

List of Tables

Abbreviations

ECMRWF	European Centre for Medium-Range Weather Forecasts
ERA5	ECMWF Reanalysis 5th Generation
LW	Longwave
MIZ	Marginal Ice Zone
NSIDC	National Snow and Ice Data Center
OI	Optimum Interpolation
SEB	Surface Energy Balance
SIA	Sea Ice Area
SIC	Sea Ice Concentration
SLP	Sea Level Pressure
SST	Sea Surface Temperature
SW	Shortwave

Chapter 1

Introduction

Within the recent satellite era, observed global temperatures have been rising. The Arctic in particular has experienced much more rapid temperature increases than the rest of the world. Recent observations show the Arctic is warming at a rate 2-3 times the trend for the rest of the Northern hemisphere, a phenomenon known as Arctic Amplification (Bekryaev et al., 2010, Box et al., 2019). At the center of this accelerated warming is the reduction of sea ice that enhances solar absorption through the albedo feedback effect (Serreze et al., 2009). Coupled with the global warming trend, is a decline in average sea ice extent in the Arctic (Carmack et al., 2015). During the summer months, the average sea ice extent has declined by over 40% since 1979 (Koyama et al., 2017, Stroeve et al., 2012). Additionally, sea ice has become thinner and younger in more recent years, making it more susceptible to further melt (Comiso, 2012, Lindsay and Schweiger, 2015). Together, these changes are beginning to define a "new Arctic," where by the end of the

century, the Arctic will be seasonally ice-free in September resulting in a host of other local climate changes. For example, due to the temperature increases, summer and fall precipitation is expected to transition from primarily snow to rain (Landrum and Holland, 2020).

At the center of the decline in ice area over recent decades is a positive feedback process supporting increased rates of ice melt. One of the defining attributes of sea ice is its high albedo, allowing for it to modulate the amount of incoming solar radiation absorbed by the surface: the more sea ice present, the more radiation reflected and less absorbed. As sea ice melts, a larger area of dark (low albedo) ocean water is exposed, allowing more radiation to be absorbed, and increasing ocean temperatures, which, in turn, causes more ice melt (Serreze and Barry, 2011). This process is summarized in Figure 1.1. This feedback cycle was particularly evident in 2007 when it proved to be an important aspect of the then record minimum sea ice extent. It has since been shown that the increase in the open water fraction in 2007 led to additional solar heat input to the upper ocean, warmer sea surface temperatures (SST), and further ice melt (Perovich et al., 2008).

Much like sea ice, clouds play an important role in modulating Arctic surface radiation. Clouds have two main effects: reflecting incoming shortwave radiation from the sun (decreasing absorbed radiation at the surface) and increasing downwelling longwave radiation from the cloud itself (increasing absorbed radiation at the surface). In the summer months when the sun illuminates the Arctic continuously, the shortwave effect tends to dominate, especially in areas of open ocean (Sledd and L'Ecuyer, 2021b). Kay
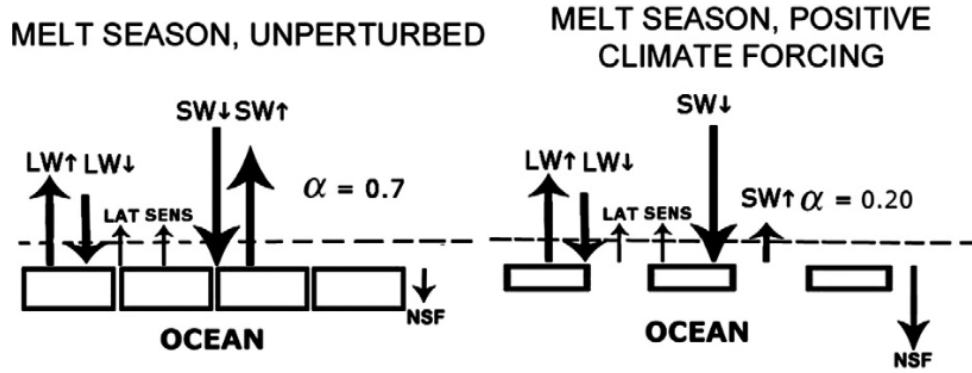
FIGURE 1.1: Summary of ice-albedo feedback (Serreze and Barry, 2011). Here the longwave (LW) and latent and sensible heat fluxes (LAT and SENS, respectively) are the same across both scenarios. The panel on the right has a much smaller upwelling shortwave (SW) response due to the lowered albedo (α) from the greater fraction of open ocean, leading to a larger net surface heat flux (NSF). This increase in NSF promotes further ice melt.

et al. (2008) show that an overall decrease in cloudiness also played an important role during the anomalously low sea ice extent year of 2007. Figure 1.2a shows how regions of decreased cloud fraction caused an associated increase in downwelling shortwave radiation and a slight decrease in downwelling longwave radiation. This larger shortwave effect caused by the presence of fewer clouds is associated with the observed sea ice extent minimum.

Conversely, over bright surfaces that already reflect most of the incoming sunlight, and during polar nights, the longwave effect tends to dominate. Van Tricht et al. (2016), for example, investigate the impacts of clouds over the Greenland Ice Sheet showing that cloudy skies lead to a positive mean cloud radiative effect that significantly increases melt and runoff from the ice sheet (Figure 1.2b). Overall, the exact role clouds play in the Arctic is still uncertain, leading to uncertainties in sea ice and Arctic temperature

---

responses to increasing carbon dioxide concentrations (Sledd and L'Ecuyer, 2021a).
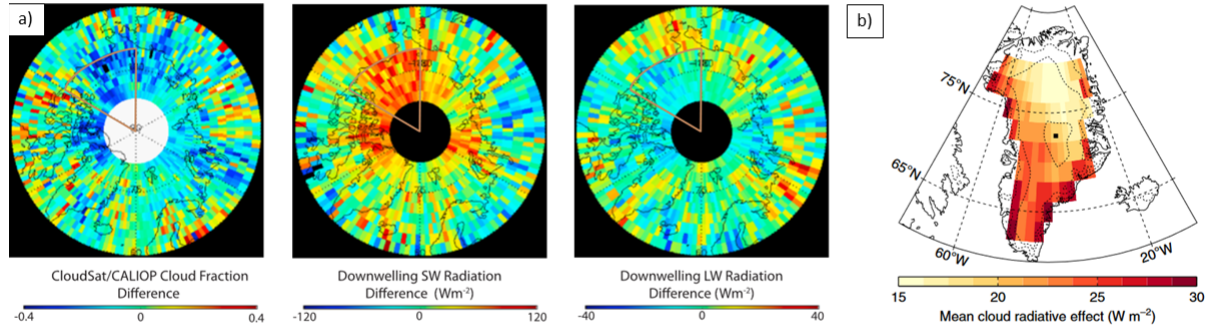
FIGURE 1.2: a) Difference in downwelling shortwave and longwave radiation between 2007 and 2006 (averaged between June 15–Sept 15) (Kay et al., 2008). A decrease in cloud fraction corresponds with an increase in downwelling shortwave (SW) radiation. b) Yearly mean cloud radiative effect over the Greenland ice sheet from 2007-2010 (Van Tricht et al., 2016). Here the presence of clouds increases the amount of downwelling radiation at the surface.

The interplay between clouds and changes in sea ice is, therefore, complicated. Because of the opposing feedback processes at play and the interdependence of cloud and ice radiative effects, the timing of the downwelling perturbations is important. Positive cloud perturbations earlier in the summer season lead to more melt by increasing downwelling longwave radiation and bringing surface temperatures closer to the melting point (Kapsch et al., 2016). Due to of the sea ice's high albedo, these longwave perturbations generally have a greater impact on melt than the accompanying shortwave, since a large fraction of the shortwave energy is reflected by the surface (Kapsch et al., 2016). However, later in the year, a decrease in cloud cover has a larger impact on melt due to the enhanced downwelling shortwave radiation and reduced albedo at the surface.

Further complicating the interplay between clouds and ice is the fact that clouds frequently occur as part of large-scale weather systems that also generate wind and precipitation that can both also influence the surface energy balance (SEB). Precipitation has the ability to alter the SEB by enhancing surface albedo. Rates of Arctic snowfall have decreased by about 40% between 1989-2009 (with the fraction of precipitation occurring as rain increasing proportionally) and because rain is much less reflective than snow, this change is also likely contributing to sea ice thinning (Screen and Simmonds, 2012). Strong winds also have the potential to contribute to a loss of sea ice area through advection. Ogi et al. (2008) show how positive sea level pressure anomalies during the summer of 2007 led to strengthened anticyclonic winds, which resulted in Ekman drift of sea ice where ice moves to the right of the surface geostrophic winds. This process then enhanced the record minimum sea ice extent of 2007 through a northward motion of ice towards the central Arctic.

In light of these considerations, one prominent aspect of the Arctic climate system that can exert a rapid influence on SEB by simultaneously altering sea ice, cloud cover, and precipitation is the presence of Arctic cyclones. These extratropical cyclones vary in size, with radii that can be as small as 50 km but extend upwards of 5,000 km, bringing along heightened wind speeds and increased precipitation (Aizawa and Tanaka, 2016). Several intense cyclones have been identified in recent years, including an extraordinary event occurring in August 2012 that greatly reduced the ice extent (Parkinson and Comiso, 2013, Simmonds and Rudeva, 2012), which has prompted considerable research in recent years to quantify the effects of cyclones on Arctic sea ice and the SEB.

Recent work into Arctic cyclones (primarily dependent on models or reanalyses) has identified them to be prominent contributors to changes in sea ice. Simmonds and Keay (2009) showed that cyclones play a role in reducing late-summer sea ice and suggested that storm intensity is more important than the overall number of storms that occur. Subsequent studies have looked deeper into this relationship, with some studies citing increased sea ice loss (Kriegsmann and Brümmer, 2014), while others claim cyclones work against the climatological decline of sea ice (Schreiber and Serreze, 2020). For example, Schreiber and Serreze (2020) found that, overall, summer storms tend to limit the seasonal decline of ice primarily through increased cloud cover. This result was supported for storms that occur earlier in the summer season, during May and June (Finocchio et al., 2020). However, Finocchio and Doyle (2021) found that late-summer storms cause slightly more sea ice loss. Additionally, the strength of the near-surface cyclonic winds also impacts the amount of sea ice loss during July and August, where storms with stronger winds are associated with greater changes in ice area than storms with weaker winds (Finocchio et al., 2020). This result is explained in part by thinner ice (which becomes more prominent later in the summer season) being more responsive to wind forcing (Kwok et al., 2013, Spreen et al., 2011). In a study of the particularly intense August 2012 storm using a fully coupled atmosphere-ocean-ice model, Stern et al. (2020) found that increased sea ice melt was caused primarily by the warm air advection caused by the cyclone, as well as an increase in turbulent ocean mixing causing enhanced bottom melt of the ice. Of course, ice gain or loss are not the only possible outcomes resulting from cyclone impacts. Cyclones can also simply redistribute the ice, with little

overall change in ice area (Clancy et al., 2022). All in all, based on these studies which heavily rely on models or reanalyses, there has yet to be a well-defined conclusion for what the net impacts of Arctic cyclones look like.

Continued comprehensive analysis of available satellite observations and reanalyses is required to untangle the multiple effects of Arctic cyclones on sea ice to better predict how these effects may change in the future. As a step toward a more complete understanding of the role Arctic cyclones play in shaping late-summer sea ice, this study examines a selection of late-summer Arctic cyclones from August and September 2007-2010 and assesses their impacts on the underlying sea ice, with special emphasis on changes in ice area within the marginal ice zone. Two individual case studies are first examined in detail revealing the different ways cyclones impact observed sea ice concentrations. Methods developed for analyzing these single cases are then extrapolated to a full census of 21 storms. While many previous studies utilize various models to define the impacts of Arctic cyclones, this study aims to utilize the complementary strengths of satellite observations and reanalyses for observing sea ice and tracking cyclones, respectively. Additionally, while many previous studies only consider short-term sea ice changes, a few days before and after the cyclone passage, this study considers ice evolution up to two weeks after the storm, revealing a possible mechanism by which storms may enhance sea ice loss by advecting it into warmer water.

Chapter 2

Data and Methods

2.1   Sea Ice

The National Snow and Ice Data Center (NSIDC) reports daily average sea ice concentrations across the Arctic on a polar stereographic grid at 25 km resolution by combining passive microwave data from three different sensors (Scanning Multichannel Microwave Radiometer, Special Sensor Microwave Imager, Special Sensor Microwave Imager/Sounder) utilizing the NASA Bootstrap algorithm (Meier et al., 2017, Peng et al., 2013).

Passive microwave emissions from the surface can be used to distinguish ice (which typically emits more microwave energy) from open ocean. Additionally, clouds do not emit

much microwave energy, allowing sea ice to easily be identified regardless of the atmospheric conditions. The NASA Bootstrap algorithm uses brightness temperature observations from the horizontally (H) and vertically (V) polarized 37 and 19 GHz channels. To determine sea ice concentration, scatterplots of observations from two of these channels are used to cluster data into open ocean and 100% ice-covered regions. Near the ice edge, the 37V and 19V channels are used since this pair is more sensitive to the ice-water boundary, and within the pack ice, the 37V and 37H channels are used. Intermediate concentrations can then be determined through interpolation between the clusters (Comiso et al., 1997). This particular algorithm is less sensitive to thin ice and layering of snow and ice, but may overlook the potential for young ice (such as grease ice or nilas) in the open water estimates. The data record ranges from late October 1978 to present.

Analyses were restricted to the marginal ice zone (MIZ), or the region of ice where sea ice concentration is between 15 and 80 percent (Strong and Rigor, 2013). Here, the largest changes are likely to occur, since lower concentration ice experiences not only surface and basal melt, but also lateral ice melt from the surrounding open ocean (Tsamados et al., 2015). Additionally, strong winds over largely open ocean regions can generate large shear fields leading to the breakdown of larger ice floes into smaller floes that are easier to advect via the same winds (Holt and Martin, 2001).

Since the cyclones analyzed here occur during the period when sea ice is naturally declining, trends due to the seasonal ice melt must be removed to isolate the influence of storms. A background climatology of sea ice area is defined as the total amount of sea ice

area within the MIZ of any analyzed storm region averaged over 2000-2019. To compare the observed changes in sea ice area during a cyclone to the background summertime melt, we define a "relative loss anomaly" metric where the 3-day climatological change in ice area is subtracted from the 3-day change for the storm year. This metric isolates the changes in sea ice due to the presence of a cyclone during a given year from the changes in ice expected in the absence of a cyclone at that time of year.

2.2 Sea Surface Temperature

To understand the environment the ice resides in, estimates of weekly mean Arctic Ocean sea surface temperature from the NOAA Optimum Interpolation (OI) algorithm are utilized (Reynolds et al., 2002). This product incorporates both in situ data (from ships and buoys) and satellite (Advanced Very High Resolution Radiometer) observations, and is provided on a 1-degree resolution global grid. Data from this product is available from November 1981 through present.

The OI algorithm is based on the methods in Gandin (1963), which converts irregularly spaced data from various sources to a regular grid. Weights for each new data input are computed from the difference between the data and the closest value in the previous week's analysis as well as the distance between the data point and the new grid point (among other factors). The weights multiplied by the difference in the data are then summed to result in an analysis increment for the new grid point, which is then added to the previous week's field to produce the new SST value.

To compare SST data to other variables over the storm time range, this data product was interpolated to the 25 km sea ice concentration grid. Doing so also allows the temperature within the MIZ to be isolated.

2.3 ECMWF Reanalyses

ERA5 reanalysis was used, specifically the 10-meter wind and mean sea level pressure products, to identify key characteristics of the cyclones analyzed (Hersbach et al., 2020). Combining models with global observations through data assimilation provides consistent data at a high spatial and temporal resolution. Pressure and wind values are based on observations collected at traditional land stations, on ships, or from buoys. The wind components also incorporate data from radiosondes, dropsondes, weather balloons, wind profilers, and aircraft-based observations. ERA5 data is available from 1950 to present day. Overall, compared with independent observations over the eastern Fram Strait, ERA5 was found to provide the most accurate wind and atmospheric profiles compared to other reanalyses (Graham et al., 2019).

Hourly mean sea level pressure (SLP) is used to identify the storm's location and duration. The SLP field was tracked over the lifetime of the storms to determine the total impact area of the cyclones.

To investigate the effects of storm-enhanced winds, hourly 10-meter winds from the ERA5 reanalysis were utilized. For this study, the hourly data were averaged to form a daily time series of wind velocity values to relate wind impacts to the daily changes in sea ice.

Additionally, like the SST product, the wind data were interpolated to the 25 km sea ice concentration grid to directly compare wind direction to changes in sea ice concentration. For further analysis, the SIC and SST fields were separated based on the prevailing meridional wind direction. This method allows for the additional investigation of the individual effects of the two wind directions.

It should be noted that the comparisons made between the meridional wind component and the changes in sea ice concentration are generalized. Ekman motion theory states surface ocean currents move at an angle (approximately 20 degrees) to the prevailing near-surface winds. This notion applies to sea ice advection. Additionally, since only the meridional component of the wind is taken into account in this study, the impact of Ekman drift is minimized as we discuss ice moving from higher to lower latitudes (or vice versa).

2.4   Clouds and Precipitation

Although a comprehensive analysis of clouds, precipitation, and radiative characteristics of the Arctic cyclones is beyond the scope of the current study, a qualitative overview of the structure of each cyclone case is examined for context. This information was provided from two satellites, CloudSat and CALIPSO. Aboard CloudSat is a 94-GHz Cloud Profiling Radar and aboard CALIPSO is the Cloud-Aerosol Lidar with Orthogonal Polarization (Tanelli et al., 2008, Winker et al., 2007). Together, these instruments

provide high-resolution vertical data for many aspects of cloud properties. The maximum latitude observed by these polar-orbiting satellites is approximately 82°N.

To better understand the cloud context of the two case studies identified, CloudSat reflectivity (from the 2B-GEOPROF product), cloud heights and phase (from 2B-CLDCLASS-LIDAR), and radiative effects of the clouds (2B-FLXHR-LIDAR) were utilized. Additionally, information from the 2C-RAIN- and SNOW-PROFILE products gave insight to precipitation intensity within the storm.

2.5   Storm Identification and Impact Area

To gain insight to the sea ice response to a variety of different cyclones, a census of storms was defined by identifying pressure minima below a threshold of 984 hPa for the months of August and September from 2007-2010.

To describe the region of impact of the storm, the daily-averaged 990 and 1000 hPa contours of the event were mapped out over the storm duration (defined as the days the storm's minimum pressure was below 984 hPa). A bounding box was then created based on the minimum and maximum latitudes and longitudes of these contours (Figure 2.1). To avoid this box becoming unreasonably wide as the storm approaches the north pole, a maximum northern latitude was defined as 85°N. Within this box, ice that is within the MIZ was identified, and winds and SST values within that region were isolated for analysis.

Overall, 24 storms were identified within the time period defined. Three cases were removed because they do not interact with the ice edge. From initial analyses, two case studies were identified to provide the framework to analyze the remaining census of storms.
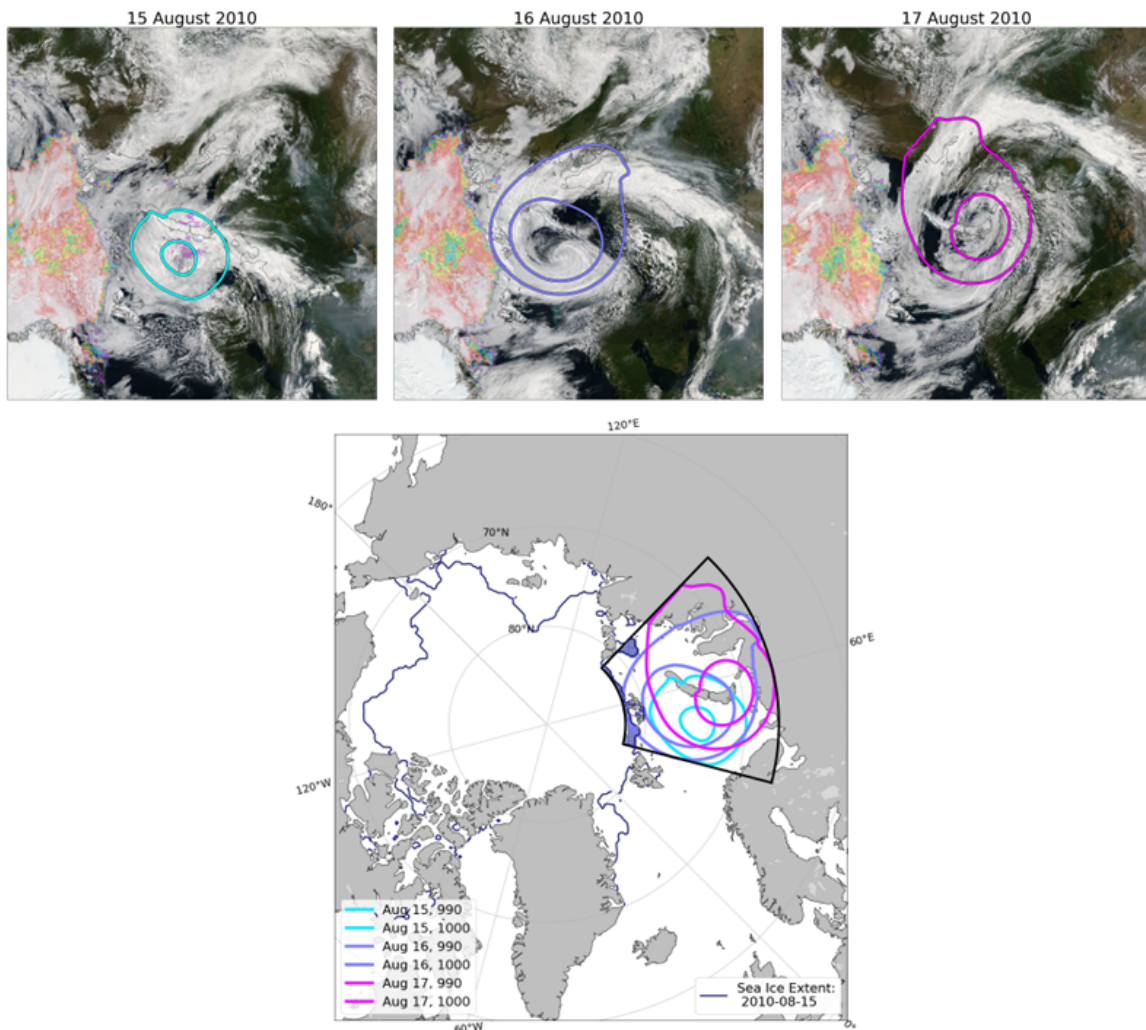
FIGURE 2.1: Top: WorldView images for August 15, 16, and 17 (left to right) with mean sea level pressure contours of 990 and 1000 hPa. Bottom: Study area for case study 1 based on the 990 and 1000 hPa pressure contours on August 15, 16, and 17, 2010. The MIZ within this study area is shaded and the sea ice extent (15% contour) for the start day of the cyclone is also plotted.

Chapter 3

Results

3.1   Case Study 1: August 15, 2010

3.1.1   Storm Development

Beginning August 14, 2010, a low-pressure minimum was identified in the Barents Sea as the initial development of an intense cyclone event. The system rapidly evolved until it became stagnant off the coast of Novaya Zemlya. At its most intense (on 16 August), the cyclone's minimum pressure was 974 hPa and maximum near-surface winds were over 23 ms^{-1}, based on ERA-5. Throughout the cyclone's lifetime, there was an advection of warm, moist air leading to the development of a thick cloud shield (Figure 3.1). As the storm matures, the cloud head thickens and the northern edge of the storm begins to overlap with the ice edge.
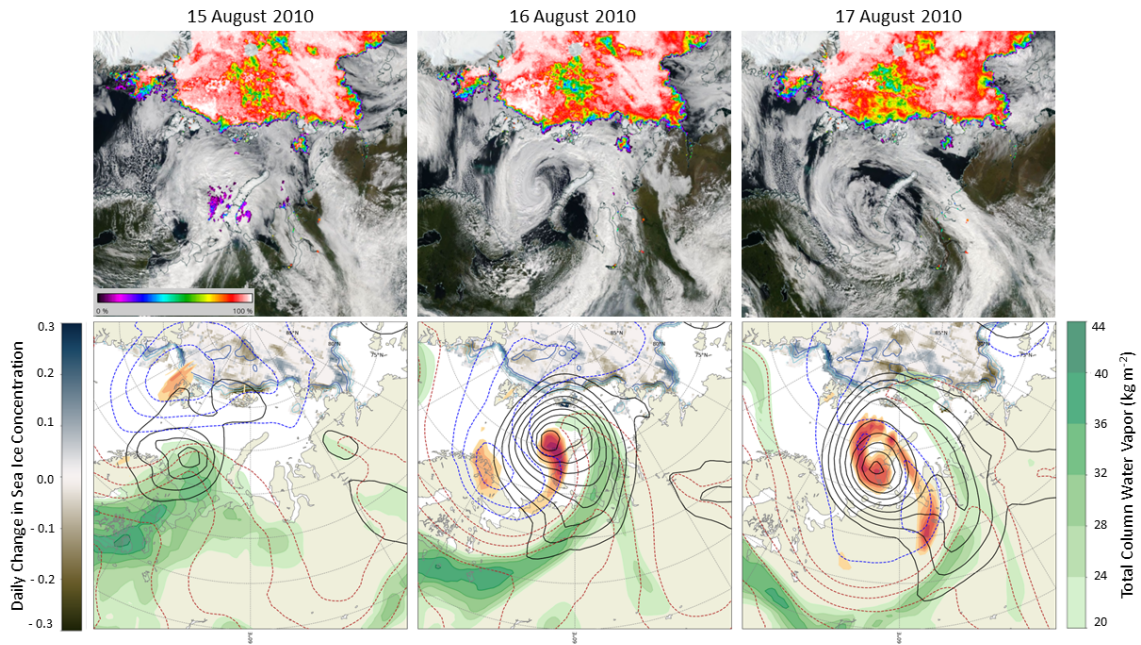
FIGURE 3.1: Each column is one day of the cyclone, ranging from August 15 through August 17, 2010. Top row shows visible images of the cyclone (Aqua/MODIS, NASA Worldview). Also depicted is the daily sea ice concentration (Aqua/AMSR-E). Bottom row shows the development of the storm with JRA-55 sea-level pressure contours (black, every 4 hPa up to 1012 hPa) and 1000-500 hPa thickness (blue/red dashed lines every 60 m). The shading consists of 500 hPa geostrophic relative vorticity (orange, every 3 x 10^{-5}s^{-1} beginning at 12 x 10^{-5}s^{-1}), total column water vapor (greens) and NSIDC sea ice concentration (contours are plotted every 20% in blue)

To gain insight into the cloud structure of this event, the vertical reflectivity and cloud phase profiles, the cloud radiative effect, and the precipitation rate are analyzed from the CloudSat overpass shown in Figure 3.2a. Based on the reflectivity in Figure 3.2b, two distinct cloud heads are identified, one central to the storm at about 72°N and another more on the periphery of the storm near 80°N. With the exception of some upper-level ice clouds and some liquid water clouds identified near the center of the storm, the clouds in this cyclone are primarily mixed phase (Figure 3.2c). This property leads to varying cloud radiative effects at the surface across this overpass (Figure 3.2d). At lower
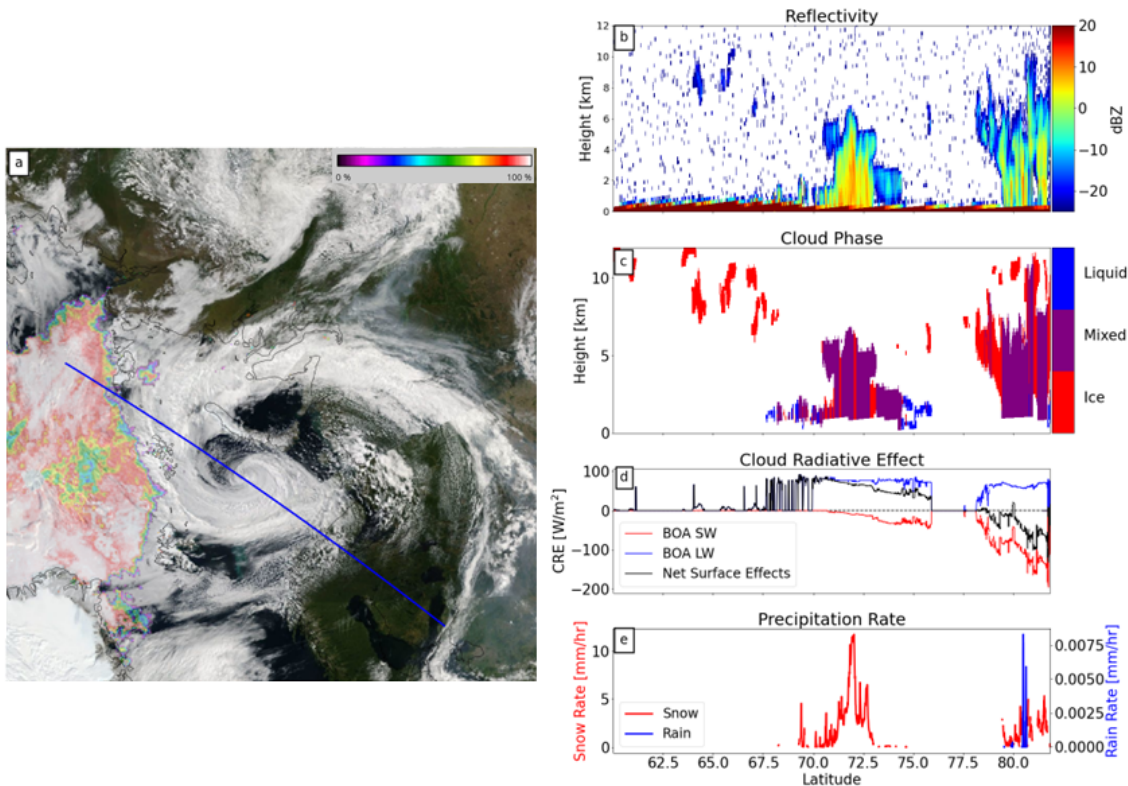
FIGURE 3.2: (a) CloudSat overpass from 2338 UTC 16 August 2010 plotted over visible imagery from Aqua (NASA WorldView). The daily sea ice concentration is also plotted. CloudSat/CALIPSO retrievals of (b) reflectivity, (c) cloud phase, (d) bottom of atmosphere (BOA) shortwave (SW), longwave (LW), and net cloud radiative effect and (e) precipitation rate along the transect in (a).

latitudes, the longwave heating effect dominates, and at higher latitudes, the shortwave effect dominates, leading to clouds cooling at the surface. The clouds over the ice, at these higher latitudes, are thicker than the clouds near the center of the storm. The thicker, more opaque clouds are more reflective allowing less shortwave radiation to reach the surface. Lastly, plotted in Figure 3.2e are precipitation rates for snow and rain. Overall, near the center of the storm, there is increased snowfall, but near the ice edge, this effect is reduced, with lower snowfall and minimal rainfall occurring. Alone, the small impact

from precipitation is likely not large enough to cause the enhanced melt discussed in Section 3.1.2, especially when coupled with the net cooling radiative effect of the clouds. However, the infrequent sampling of CloudSat and CALIPSO makes it impossible to confirm this statement for any individual cyclone case. A more comprehensive statistical analysis of several cases will be conducted in the future to better quantify these effects.

3.1.2 Sea Ice Analysis
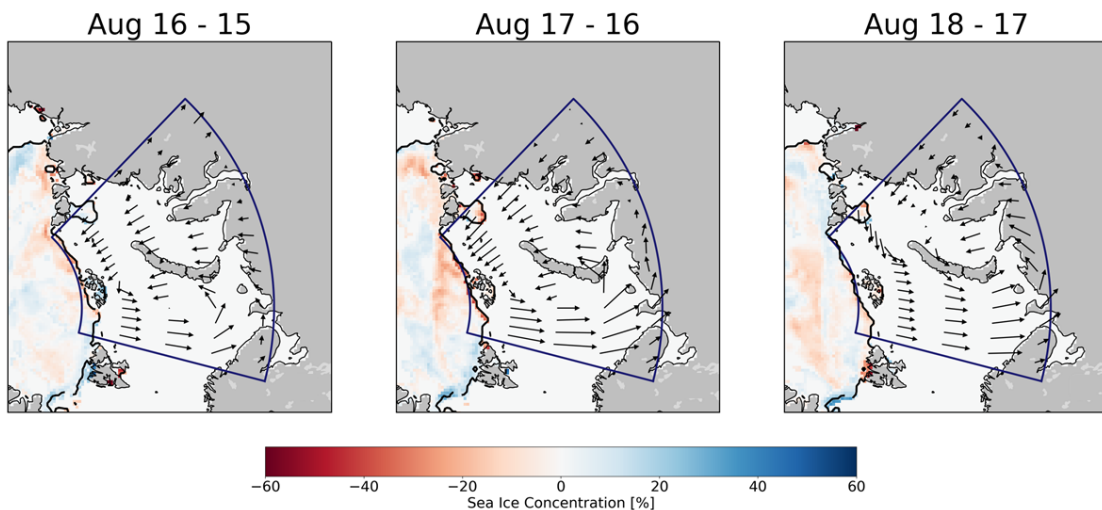
FIGURE 3.3: Change in sea ice concentration over the three days of the storm. Wind vectors are plotted within the pre-defined storm area.

As shown in Figure 2.1, this cyclone developed right along the southern edge of the ice pack. In total, within the storm impact area, there was only 35,150 km^2 of ice on the first day of the storm (15 Aug), with almost all of this ice (35,056 km^2) within the MIZ. Figure 3.3 shows the daily change in sea ice concentration across the three days of the storm. Along the ice edge within the pre-defined box (particularly during the second day
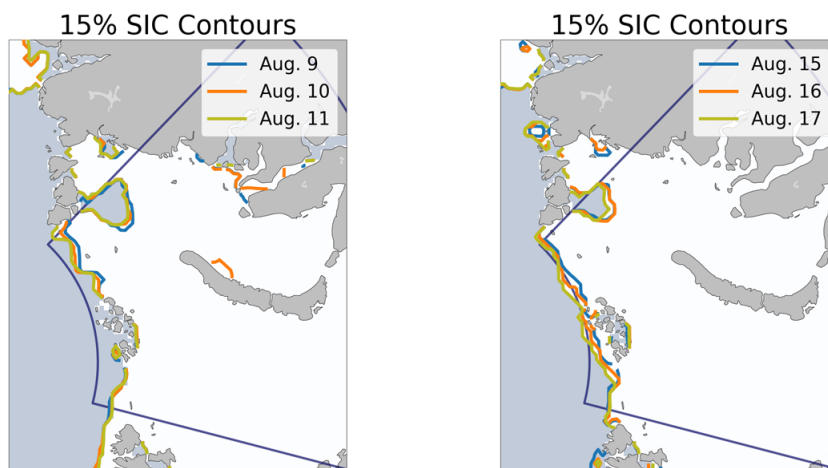
FIGURE 3.4: Ice extent (15% sea ice concentration contour) within the week prior to the storm (left: August 9, 10, and 11) and for the three days of the storm (right: August 15, 16, and 17).

of the storm), there is largely a decrease in the ice concentration. Also, the ice edge shows evidence of retreat. On the first day, there is ice along the entire northernmost boundary of the box. However, by the third day, only a portion of the boundary intersects with the ice edge. The retreat of the ice edge is shown in Figure 3.4.

The time series of ice area within this region from a week before the storm start to two weeks afterward is presented in Figure 3.5a. The most drastic change occurs in the week leading up to the storm. As shown in Figure 3.4, this result is likely due to the seasonal loss of coastal ice, as the edge of the northernmost ice remains mostly constant leading up to the storm. However, during the storm (shaded), there is a net decrease in ice within the MIZ of 12,587 km^2. This loss of ice is 5,750 km^2 more than the climatological average 6,837 km^2 loss expected during this time of year, as predicted from the observed average of ice areas within this region from 2000-2019 (Figure 3.5).
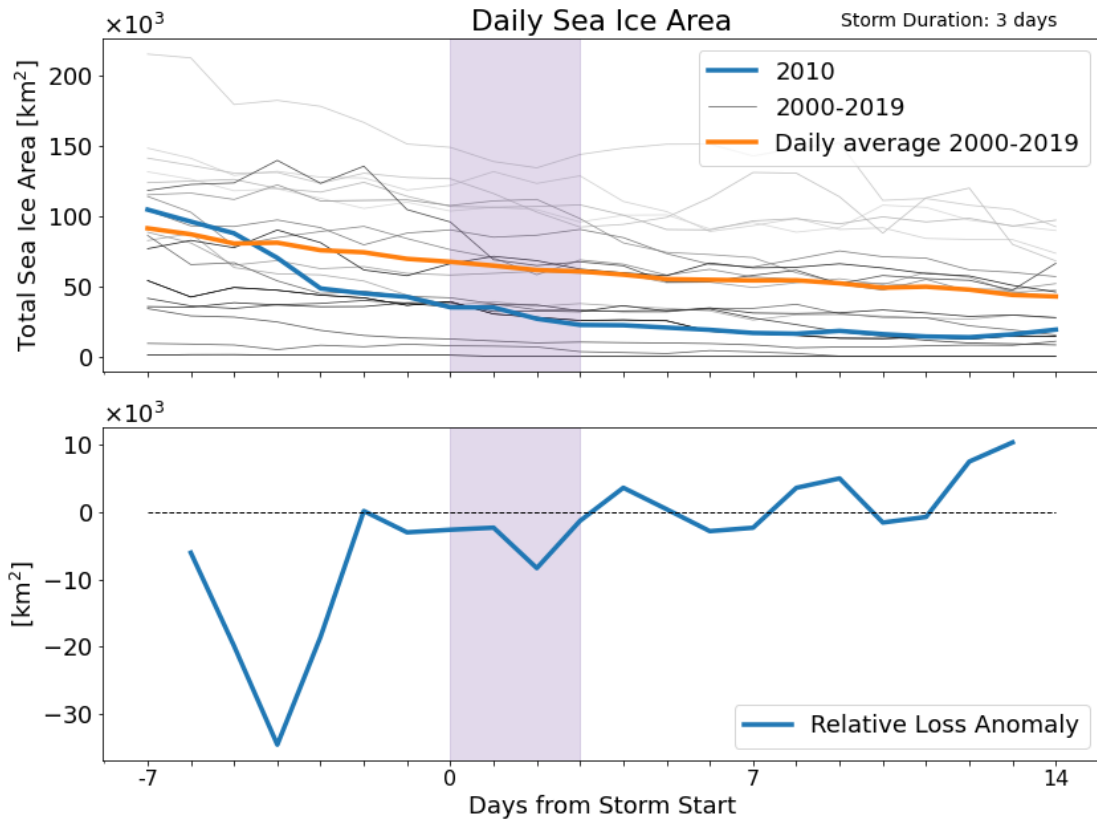
FIGURE 3.5: (a) Daily sea ice area averages from 2010 (blue) as well as a climatological average from 2000-2019 (orange) for the study area defined in Figure 2.1. Gray lines show the individual years that make up the climatology, with darker colors indicating more recent years. (b) Difference between the 2010 and climatological area anomalies.

The comparison of the amount of sea ice lost or gained between the storm year and the climatological average is shown in the relative loss anomaly curve (Figure 3.5b). During the storm (shaded), the relative loss anomaly is negative, indicating that the cyclone is causing more rapid ice loss than what would otherwise be expected due to the seasonal melt. Recall that the relative loss anomaly considers three-day averages, such that the trend over the full storm duration is considered, rather than day-to-day variability.

Shortly after the storm, the relative anomalies oscillate around zero. So while the total ice area is much smaller than the climatological total and continues to decline after the storm, it is at a similar rate to the average background melt. To better understand the mechanism driving this enhanced melt during the storm, the thermodynamic and mechanical aspects of the storm (specifically the meridional winds) and its environment (SSTs) were considered.

3.1.3 Analysis of Winds and Sea Surface Temperature

Figure 3.3 highlights two potential avenues for ice loss. During the storm, enhanced winds associated with the storm dynamics may move ice (potentially out of the analysis domain) or compress it. Through this advection process, the sea ice is driven into different temperature water. Generally, there is a meridional temperature gradient, so as ice moves southwards it moves into warmer waters, which has the potential to enhance ice loss long after the storm passes. Alternatively, northward transport of ice is associated with a decrease in SST which leads to potential slowing of ice melt. Meridional wind and SST values were isolated within the MIZ and compared over the lifetime of the cyclone to examine these effects.

The development of the storm's near-surface winds for 15-17 August 2010 overlaid on sea ice concentration changes relative to the day prior is shown in Figure 3.3. As expected, the western side of the cyclone is dominated by northerly winds and the eastern side is dominated by southerly winds. Interestingly, this produces a dipole-like structure within the sea ice concentration difference during most days, where along the coast there are

regions of decreasing concentration immediately adjacent to regions of increased concentration. In locations with on-ice flow, there is a local loss of ice denoted by a negative change in sea ice concentration. On the opposite side (with off-ice flow), there is an initial increase in concentration during the first day of the storm. This slight gain in ice has the potential to partially offset the other impacts of the storm. During the later days of the storm, however, the region on the western side of the cyclone experiences a decrease in concentration.

To begin to quantify the qualitative story presented above, the winds over the MIZ were averaged for each day (Figure 3.7a). During this event, the northerly winds dominate over the sea ice, associated with the southward advection of ice and an initial increase in concentration. The northerly winds also persist long after the storm has passed and the ice area decreased.

Furthering this analysis, the SST in the vicinity of the MIZ was examined. Figure 3.6 shows the evolution of the MIZ throughout the storm overlaid on the regional SST values. Right before the storm, the MIZ is shifted only slightly northwards relative to a week prior, likely due to the expected seasonal retreat. However, during the storm, much of the marginal ice on the eastern side of the storm is advected out of the analysis area. On the western side, there is a slight increase in area, where the extent of the ice edge briefly exceeds the ice extent from a week prior, reaching into a region of warmer SST. One week after the storm, that extended area has receded.
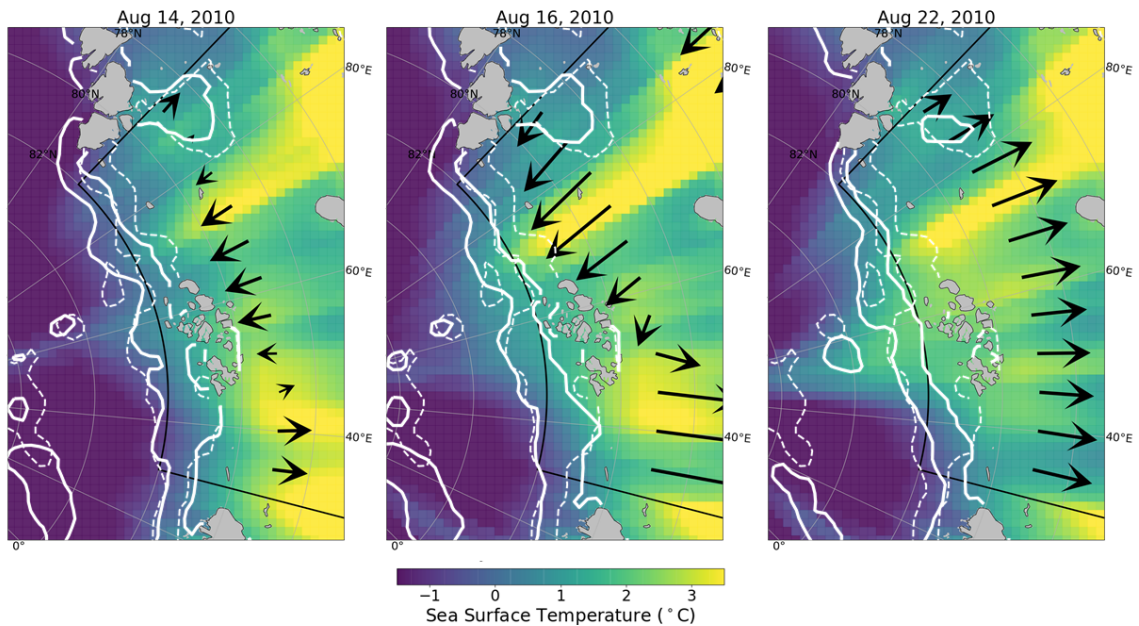
FIGURE 3.6: Sea surface temperature within the MIZ for one day before the storm (left), one day into the storm (middle), and one week after the storm's start date (right). Solid lines depict the current 15% and 80% concentration contours. Dashed lines depict the MIZ from one week prior to the storm (August 8, 2010). Daily-averaged 10-meter winds are also shown.

Quantifying these results, Figure 3.7b presents daily average SSTs within the MIZ. As shown in Figure 3.6, because of the wind advection, the marginal ice zone is not static over this time, so Figure 3.7b shows specifically the temperature where the ice is located during each day. Within the storm days, the overall sea surface temperature is steadily increasing. It even remains high for over a week after the storm. These SST changes are confirmed in Figure 3.7c, which shows positive SST changes leading up to and during the storm event. Overall, the changes occurring during this storm period are not more anomalous than in other periods, though the trends are still present.
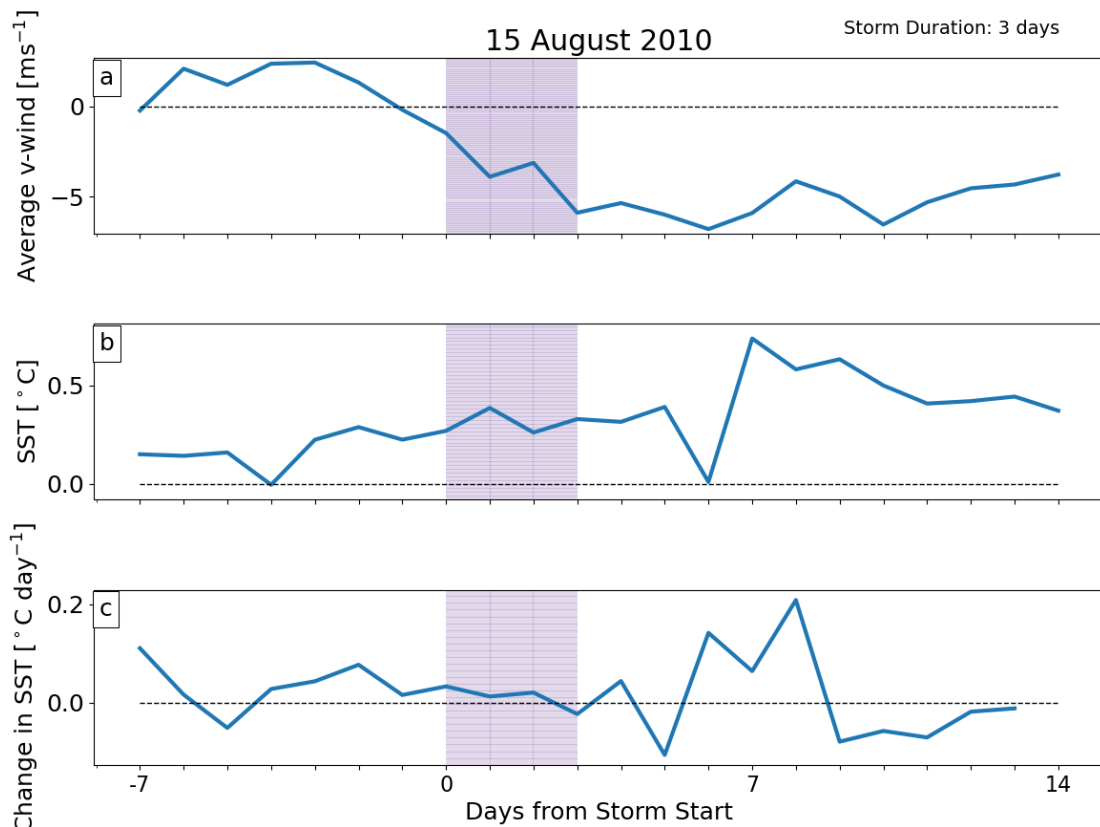
FIGURE 3.7: (a) Average wind velocity within the MIZ from one week before the storm through two weeks after. During the storm event (shaded), the ice is dominated by northerly winds causing southward advection of ice. (b) Average SST within the MIZ from one week before the storm through two weeks after. (c) 3-day derivative of (a). During the storm the SST is increasing, as shown through the positive derivative, and remains high (above-freezing) for over one week after the storm dissipates.

3.1.4 Wind Separation Analysis

Although the northerly winds prevail, both the southerly and northerly winds play an important role in modulating sea ice during this event. To gain a clearer understanding of these opposing wind effects, the ice areas with northerly winds and southerly winds were separated during the main storm days. Then, the daily sea surface temperature and daily sea ice area were calculated within the regions of northerly and southerly winds during
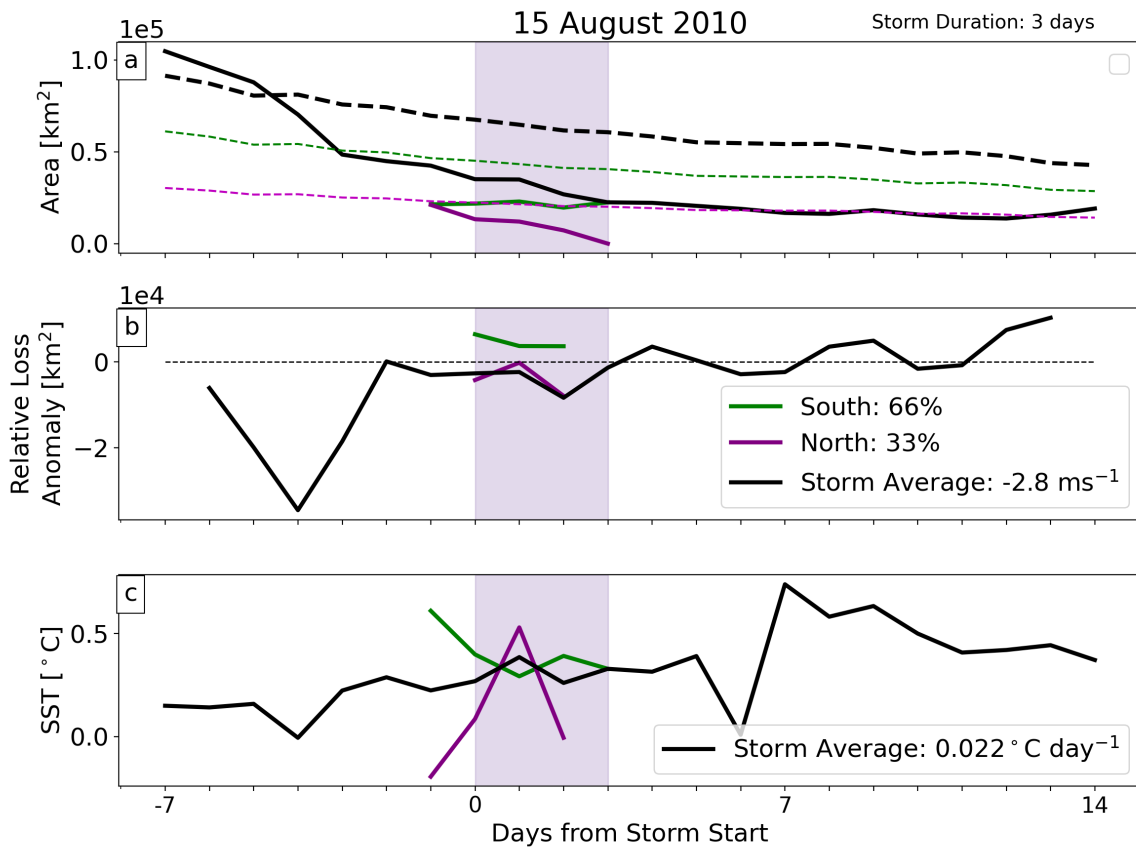
FIGURE 3.8: Separation by wind region for (a) sea ice area (dashed lines show respective climatologies), (b) area relative anomaly, and (c) SST. During the storm, southward winds dominate in both magnitude and area, where about two-thirds of the ice area was experiencing southward winds and one-third was experiencing northward winds. These southward winds are associated with an increase in area, whereas the northwards winds are associated with a decrease in ice area.

the storm. These values are plotted in Figure 3.8. During the storm, there is a slight increase in the southward ice area, as the northerly winds advect the ice into the open ocean, and a decrease in the northward area, as the southerly winds compress the ice. By the end of the storm lifetime (shaded), all the ice experiencing northward-flowing winds was advected out of the analysis domain such that all the ice remaining was experiencing southward forcing. As for SST trends, the marginal ice under the influence of southward

winds experiences a decrease in SST and the marginal ice under the influence of northward winds experiences an initial increase in SST followed by a decrease. In this scenario, the ice is likely moving from a region of cooler SST to warmer SST. Alternatively, a potential cause of this increase in SSTs around the ice edge is through the enhanced mixing at the atmosphere-ocean interface driven by the enhanced cyclonic winds, leading to an upward flux of oceanic heat (as described in Zhang et al. (2013)).

Overall, there is a noticeable decline in the marginal ice zone area during this storm. This result is likely driven by the prevailing northerly winds which cause the ice to move southward into warmer waters. This one cyclone event sets the stage for other cyclones with dominant winds that cause ice to move into warmer waters. On the other hand, some storms may have the potential to have the opposite effect, where the prevailing winds cause a decrease of SST within the MIZ leading to a potential for ice growth (or a slowing of the seasonal melt).

3.2   Case Study 2: August 25, 2010

3.2.1   Storm Development

This second storm occurred a little over a week after the initial case study analyzed but in a different location, in the East Siberian Sea. Starting to develop on August 25, 2010, this storm quickly took a different form than the previous case study. Overall, there is less moisture transport leading to a less well-defined cloud structure (Figure 3.10). At
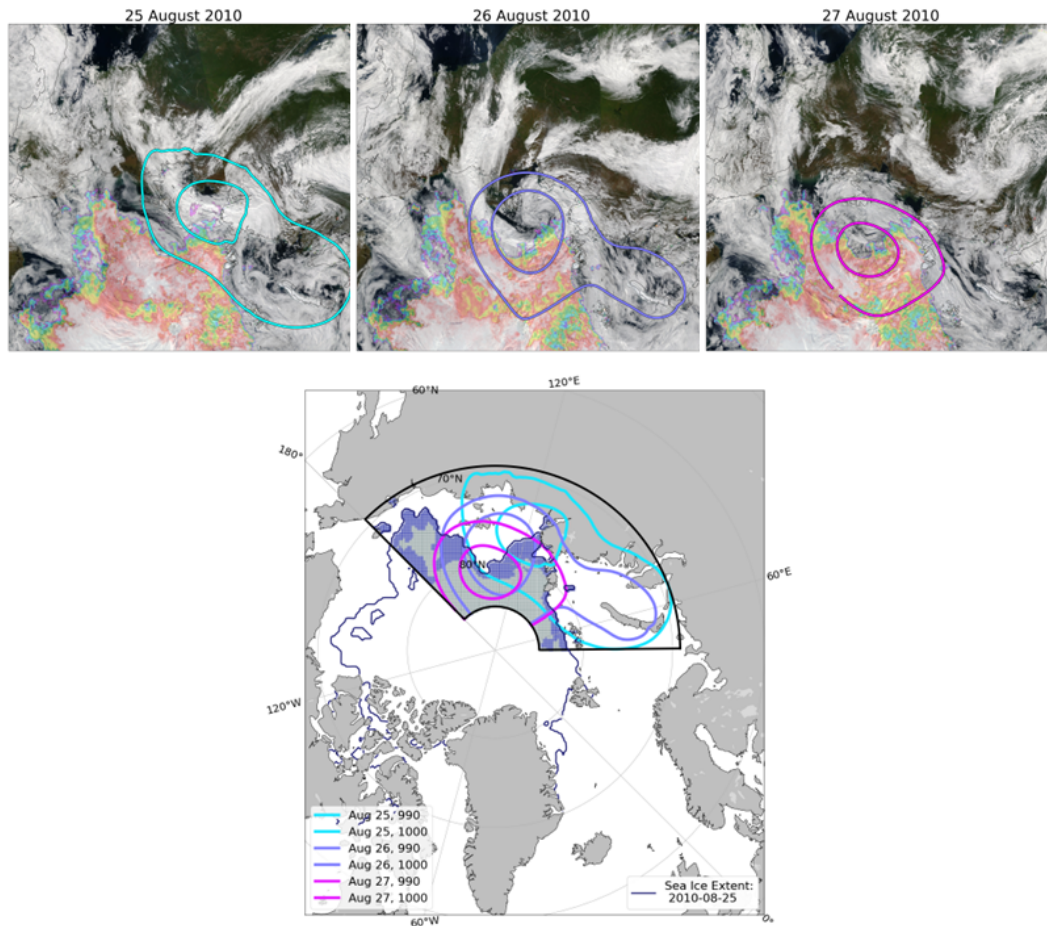
FIGURE 3.9: Top: WorldView images for August 25, 26, and 27 (left to right) with mean sea level pressure contours of 990 and 1000 hPa. Bottom: Study area for case study 2 based on the 990 and 1000 hPa pressure contours on August 25, 26, and 27, 2010. The MIZ within this study area is shaded and the sea ice extent (15% contour) for the start day of the cyclone is also plotted.

its peak, this storm reached a minimum pressure of 976 hPa and had maximum winds reaching upwards of 20 ms^{-1}.

This storm also behaves differently from a cloud and precipitation perspective (Figure 3.11). At lower latitudes, there is a much taller and more prominent cloud head in this second case, though the clouds are also primarily mixed-phase. Closer to the ice
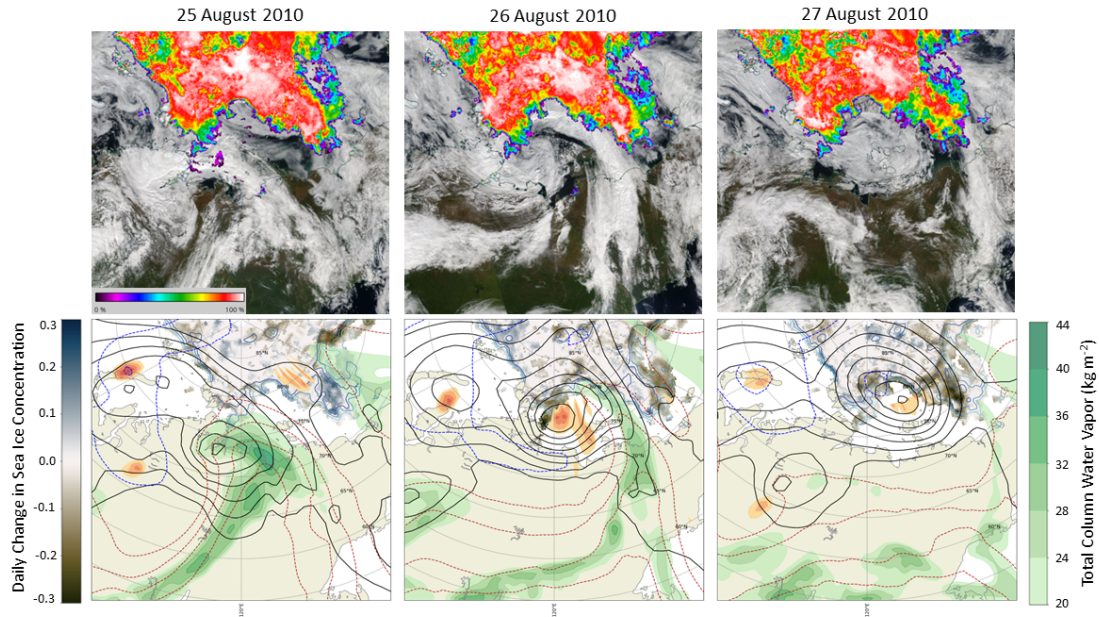
FIGURE 3.10: As in Figure 3.1, but now each column ranges from August 25 through August 27, 2010.

edge, at higher latitudes, the clouds become much shallower (especially relative to the first case). Additionally, there is a greater amount of liquid water clouds over the ice in this case. Overall, throughout the full transect, the net radiative effect from the clouds is negative, leading to cooling near the surface. There is also persistent snowfall throughout much of the transect. Both of these qualities have the potential to help promote ice growth.

3.2.2 Sea Ice Analysis

The impact area of this storm is shown in Figure 3.9. Overall, this storm interacted with a much larger area of ice (1,268,081 km^2 on the first day of the cyclone event, about 36 times the area of Case 1). Additionally, in this case, only 372,931 km^2 of ice lies within
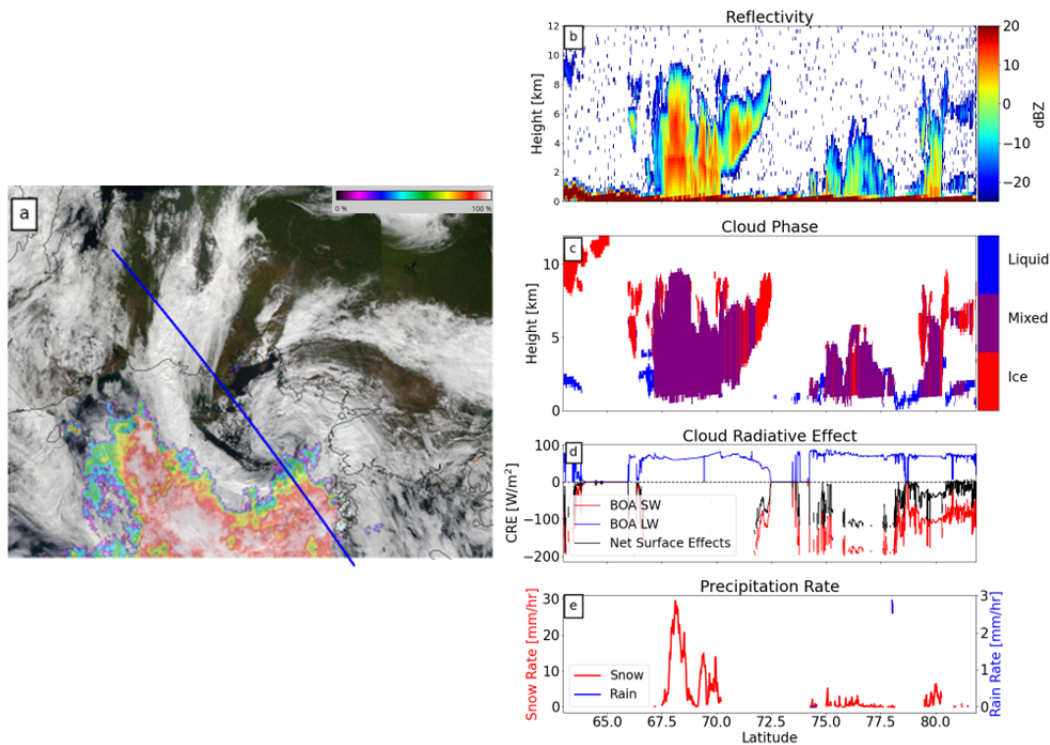
FIGURE 3.11: (a) CloudSat overpass from 0111 UTC 26 August 2010 plotted over visible imagery from Aqua (NASA WorldView). The daily sea ice concentration is also plotted. CloudSat/CALIPSO retrievals of (b) reflectivity, (c) cloud phase, (d) bottom of atmosphere (BOA) shortwave (SW), longwave (LW), and net cloud radiative effect and (e) precipitation rate along the transect in (a).

the MIZ, or about 30% of the total ice area within the study region. This larger area is partly due to the neighboring low pressure to the west of the main cyclone center which expands the area of the 1000 hPa contours, particularly on the first two days of the storm.

Figure 3.12 shows the daily changes in sea ice concentration. Like the first case, there is a strong dipole structure, where the eastern side of the storm experiences a decrease in sea ice concentration and the western side experiences an increase, matching the direction of forcing from the winds. Unlike the first case, there is not as much of an obvious change in the overall extent of the ice edge. The 15% sea ice concentration contour plotted in
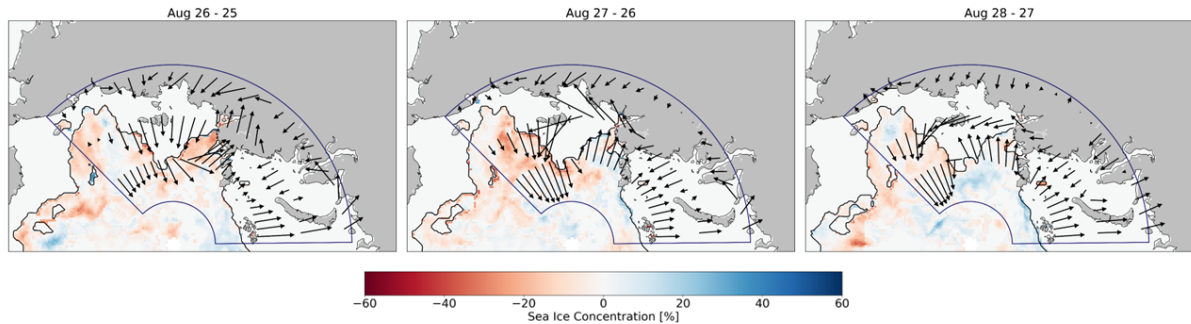
FIGURE 3.12: Change in sea ice concentration over the three days of the storm. Wind vectors are plotted within the previously defined storm area.

Figure 3.12 remains roughly static over the three main days of the storm. This result is shown again in Figure 3.13, where most of the changes in the MIZ over the duration of the storm occur in along the 80% contour instead.

The time series of ice area within this region from a week prior to the storm start to two weeks afterward is presented in Figure 3.14a. There is not an obvious decline in ice, as there was in the first case. In fact, during the shaded storm period, there was a net gain of 46,600 km^2 of ice within the MIZ, while based on the mean climatology, about 34,490 km^2 of ice loss was expected. Throughout the storm days, the relative loss anomaly is positive, indicating that there is more ice gain than expected within the storm area compared to climatology (Figure 3.14b).

To compare this result with the previous case study, the same analysis of winds and sea surface temperature was performed.
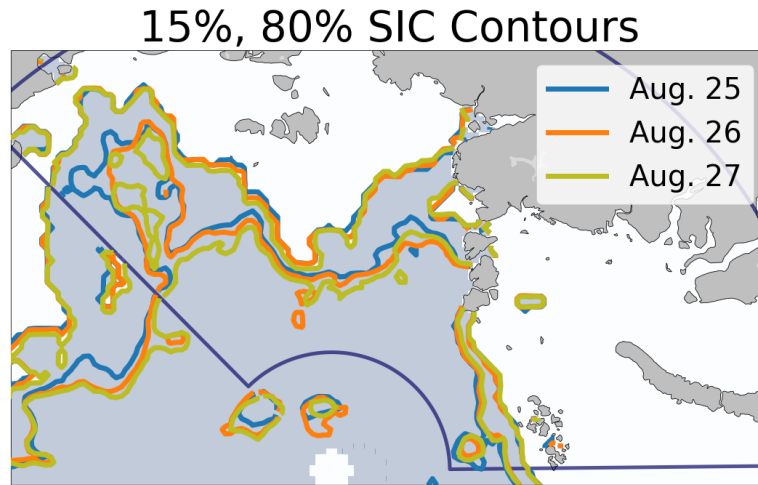
FIGURE 3.13: Marginal ice zone (15% and 80% sea ice concentration contours) for the three days of the storm.

3.2.3   Analysis of Winds and Sea Surface Temperature

Figure 3.12a-c shows the evolution of the winds from 25-27 August 2010 atop changes in sea ice concentration. Similar to Case 1, on the western side of the storm where there is off-ice flow, there is an increase in ice concentration as the marginal ice is advected into the open ocean. Overall, within the marginal ice zone, the wind pattern is predominantly northwards, which is confirmed in Figure 3.16a, which shows the daily average wind values within the MIZ. As previously mentioned, the weakened southward flow on the western side could be related to the lack of an upstream anticyclone and instead an adjacent low-pressure system following the cyclone.
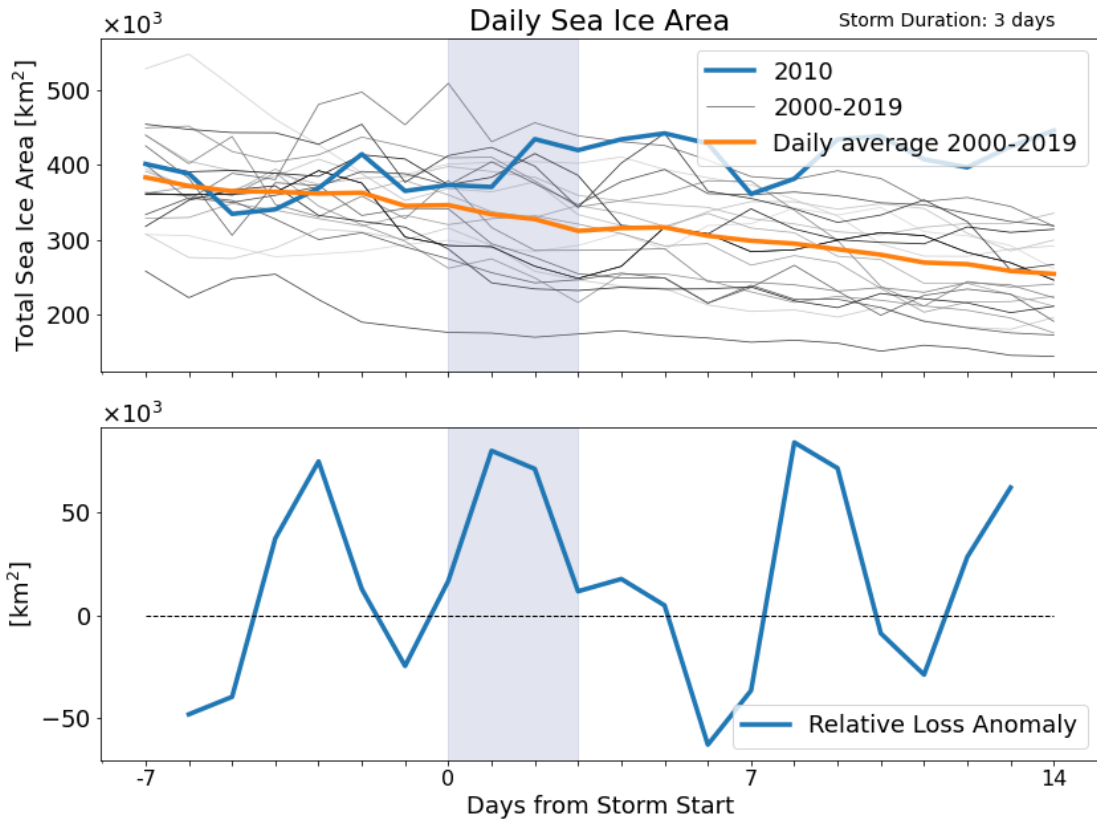
FIGURE 3.14: (a) Daily sea ice area averages from 2010 (blue) as well as a climatological average from 2000-2019 (orange) for the study area defined in Figure 3.9. Gray lines show the individual years that make up the climatology, with darker colors indicating more recent years. (b) Difference between the 2010 and climatological area anomalies.

To better understand the impact of the northward advection of ice, SST values within the region of the storm are shown in Figure 3.15. Right before the storm, the MIZ is fairly similar to the MIZ of the week prior, except for a slight northward retreat. However, two days later, at the height of the storm, there is an evident retreat of the 80% contour within nearly the entire storm area, causing the MIZ to widen and increase the area of ice it contains. After the storm, the MIZ remains relatively wide, and because of this change, the larger area of marginal ice resides in regions of cooler SST closer to the pole.
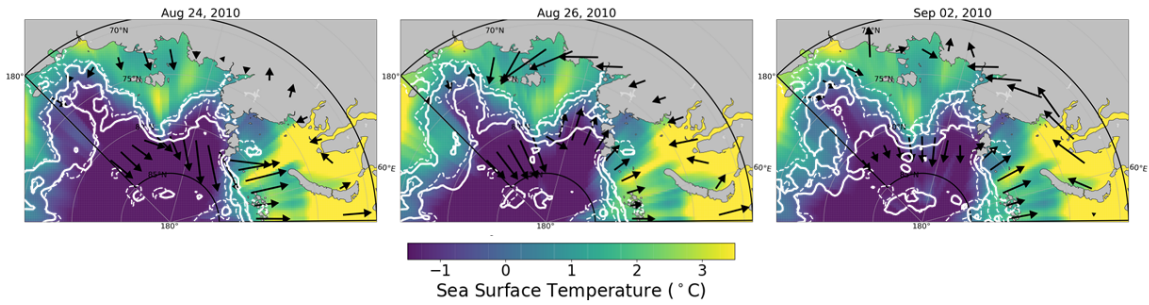
FIGURE 3.15: Sea surface temperature within the MIZ for one day before the storm (left), one day into the storm (middle), and one week after the storm's start date (right). Solid white lines depict the current 15% and 80% concentration contours. Dashed white lines depict the MIZ from one week before the storm (August 18, 2010). Daily-averaged 10-meter winds are also shown.

The time series of daily SST values within the MIZ is then plotted in Figure 3.16b. Prior to the storm, the SST within the MIZ was fairly constant around 0.75°C. Then during the storm, there is a decline in the temperatures (Figure 3.16c plots the rate of change of the SSTs and shows a switch from near-zero to negative changes during the storm). On average, the dominant northward winds compress the ice poleward where there are cooler SSTs. These results are opposite the storm conditions of the first case, which is dominated by winds advecting ice southwards, which then causes the ice within the MIZ to reside in warmer waters.

3.2.4   Wind Separation Analysis

Applying a similar separation of northerly and southerly wind regimes as Case 1, we find that it is the northward advection of ice that is responsible for most of the increase in ice area within the MIZ (Figure 3.17a). The relative anomaly plot (Figure 3.17b) shows a more rapid increase in area for the ice under the influence of northward-flowing winds
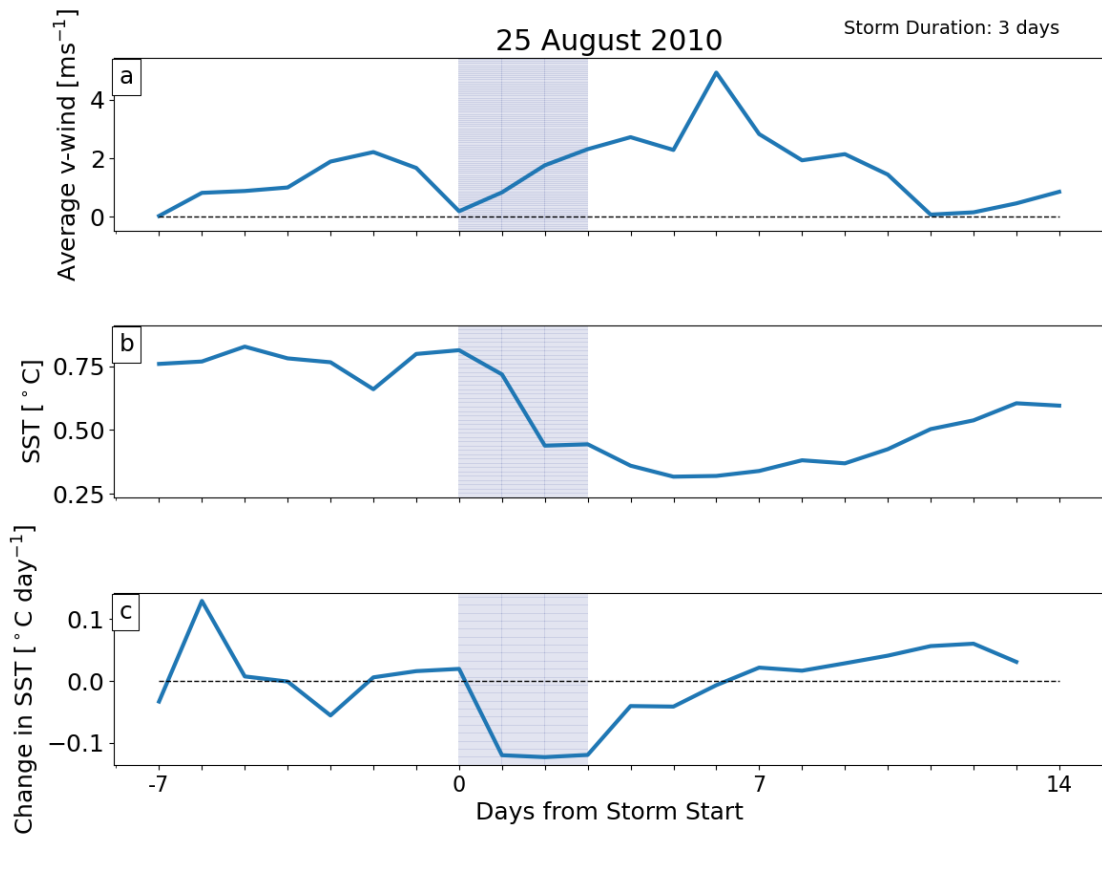
FIGURE 3.16: (a) Average SST within the MIZ from one week before the storm through two weeks after. (b) 3-day derivative of (a). During the storm the SST is decreasing, as shown through the negative derivative.

than southward. Finally, both regions experience a decrease in SST during the storm (Figure 3.17c).

In the first case, the southerly winds resulted in a decrease in area, likely due to a combination of ice compression, retreat out of the analysis region, and advection of ice into regions of higher SSTs, as opposed to the increase in ice area shown in this case which is associated with a decrease in SST. The dominant southerly winds in this case cause a retreat of the 80% contour, causing the MIZ to widen and corresponds with the increase

in area. This newly expanded area extends into the region of cooler SSTs. Overall, the results of this case are much different than those of the first cyclone event analyzed. These two drastically different responses illustrate the wide variety of ice behaviors possible due to intense summer cyclones, potentially explaining the range of results present in current literature.
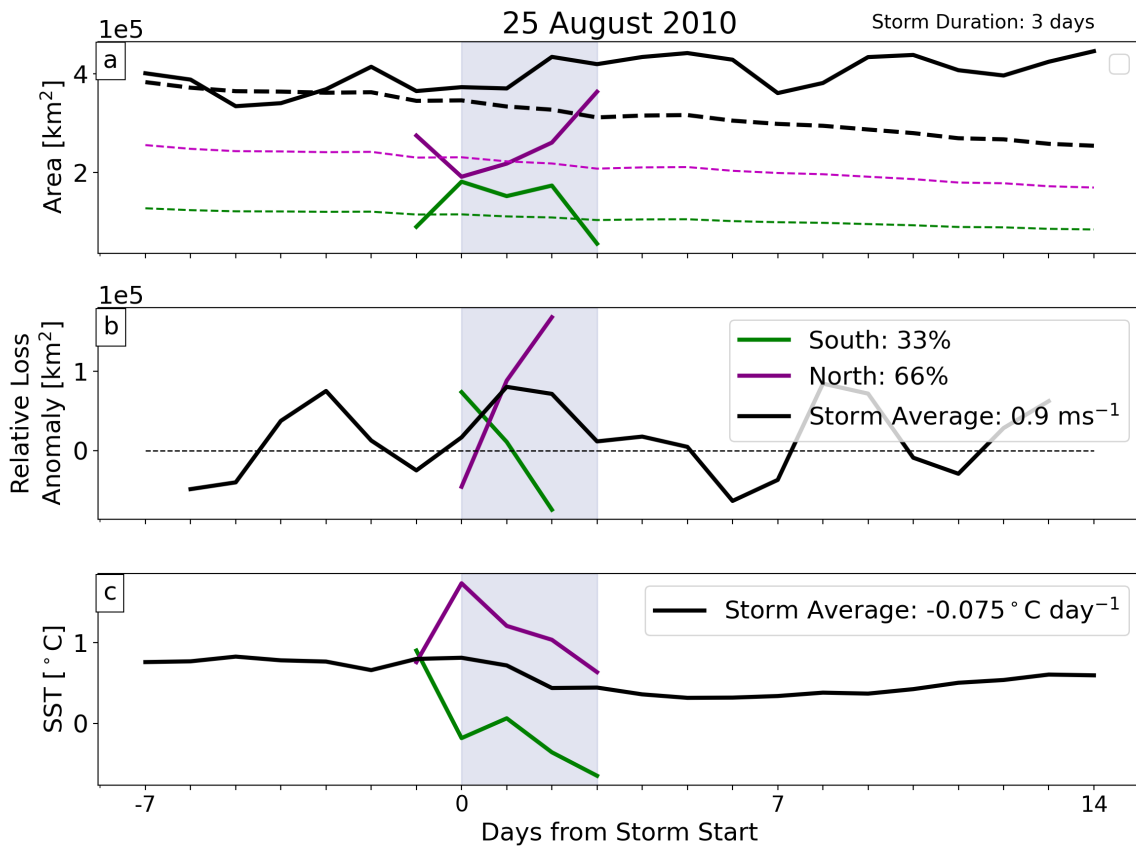
FIGURE 3.17: Separation by wind region for (a) sea ice area (dashed lines show respective climatologies), (b) area relative anomaly, and (c) SST. During the storm, northward winds dominate in both magnitude and area, where about two-thirds of the ice area was experiencing northward winds and one-third was experiencing southward winds. These northward winds are associated with an increase in area.

3.3 Composite Analysis

3.3.1 Categorization of Storm Responses

To further explore this range of responses, a method is developed for categorizing and compositing storms. By averaging together storms with similar characteristics, the variations in wind and SST curves are minimized and a clearer picture of the ice response emerges. One primary relationship that was identified was based on the analysis of these two case studies is the one between wind direction and sea surface temperature. In the first case study (August 15, 2010), an overall decrease in sea ice in the region of the cyclone was observed coupled with both an increase in northerly winds and an increase in sea surface temperature within the MIZ, leading to a localized increase in ice area while the northward advection causes a localized decrease in area. The proposed ice loss mechanism is that the winds advect the sea ice southward into warmer waters causing increased melt during the storm. However, this behavior is not always observed. The second case study analyzed (August 25, 2010) illustrates ice response in a storm dominated by southerly winds. In this case, there was an increase in ice area within the MIZ, accompanied by a decrease in sea surface temperature. These two case studies provide the basis for potentially categorizing cyclone behaviors with respect to wind direction and SST change in the MIZ.

Expanding on these two case studies, a census of 21 August and September storms observed between 2007 and 2010 was analyzed to generate a composite picture of how sea

ice responds to late-summer cyclones. The 21 cyclones were divided into four categories based on their dominant wind direction (northerly or southerly) and sea surface temperature trends (warming or cooling) in attempt to distinguish storms that decrease ice area from those that increase it or simply redistribute it but have little net impact.

Table 3.1 shows the breakdown of storms in each category. Overall, out of the 21 total storms, 5 match the forcings of the first case study, and 2 match the forcing of the second case study. Out of the remaining 14 storms, 9 storms have mostly southward winds but experience a decrease in SST values within the MIZ and 5 storms have mostly northward winds but experience an increase in SST values within the MIZ.

Storm Category	Count
Southward winds, Increasing SST	5
Northward winds, Decreasing SST	2
Southward winds, Decreasing SST	9
Northward winds, Increasing SST	5
Total	21

TABLE 3.1: Categorization of storms based on dominant wind direction and SST trends during the cyclone event.

3.3.2 Composites

To summarize the variations that exist within these categories, composite time series are shown in Figure 3.18. The time series analyses of sea ice area, average meridional wind, and SST within the MIZ, that were demonstrated in Sections 3.1 and 3.2 were applied to all storms in a single category and averaged. To account for differences in total ice area from case to case, ice area trends are plotted as a fraction of the total at the start of the

time series. Likewise, SST trends are shown as changes relative to the starting SST one week prior to the start of each storm.
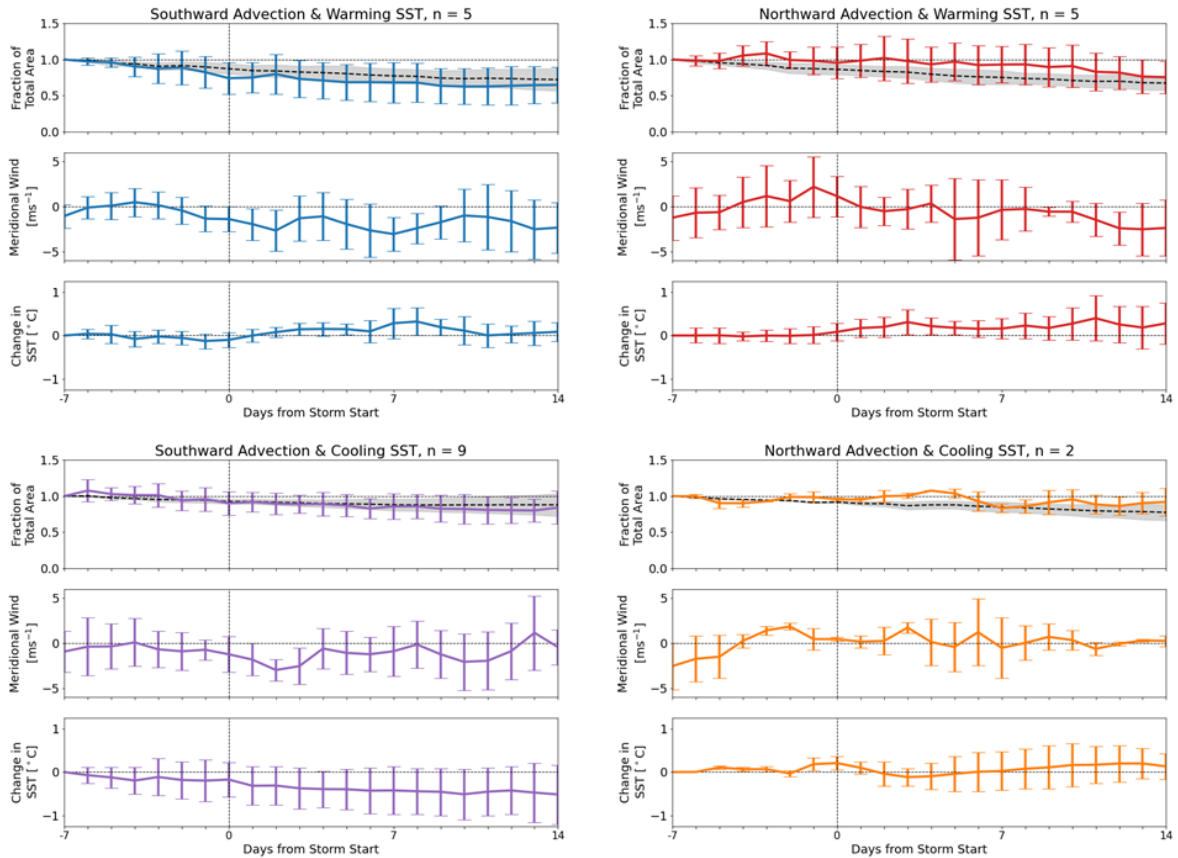
FIGURE 3.18: Composite trends for all identified August and September storms from 2007-2010 separated into 4 categories based on dominant wind direction and sea surface temperature trends. The left column shows storms with mostly southward-advecting winds and the right column shows storms with mostly northward-advecting winds. The top row shows storms with increasing SSTs and the bottom row shows storms with decreasing SSTs. Within each subplot, the top plot is the fraction of sea ice area relative to the starting area, the middle plot is average meridional winds, and the bottom plot is the change in SST relative to the temperature one week before the storm, all within the MIZ. The dashed lines show the average climatological melt for all storms within the category. Error bars represent one standard deviation across the storms in each category.

The top left plot (blue) shows the trends for the five cases that match the initial case study analyzed. Here there is a strong downward trend in sea ice area that is more rapid

than the average climatological decline in the regions of these storms. Additionally, there are well-defined trends in the southward winds becoming stronger within a few days of the storm start times, as well as a clear increasing trend in the SST anomaly continuing up to a week after the storm.

The category containing the second case study and one other storm (lower right plot, orange) shows a slight increase in sea ice area within the MIZ lasting up to a week after the storm start. The sea ice area then declines post-storm, returning to values similar to and slightly above climatology. Leading up to the storm start, the winds become more southerly and remain so throughout the average storm duration (about three days). After the storm, the winds become much more variable with a large spread in values. As for the SST values, there is little to no change until about two days prior to the storm where there is a slight increase in values, followed by a decreasing trend through the typical storm duration. Like the wind values, immediately post-storm, the spread in SST values become quite large. The large spread in wind and SST values can partially be explained by the small sample size in this category.

The cases experiencing primarily northwards winds and an increasing SST trend (upper right plot, red) do not have a clear sea ice area trend. The mean ice area fraction stays around one for most of the time period analyzed, with a large spread in values. Here, the average trend in these five storms is to work against the climatological decline in sea ice. Much like the previous case, the winds become more southerly leading up to the start of the storm and then decrease in magnitude throughout the storm. Overall, there is a large

spread in these five storms' wind characteristics throughout the time period analyzed. The SST trends are also similar to the previous category. In the week leading up to the start of the storm, there is virtually no change in SST. However, after the start of the storms, there is a clear warming trend. The heightened SST values persist through the full two-week time period analyzed after the storm.

Finally, like the first category discussed, the category defined by primarily southward advection and a cooling SST trend (bottom left, purple) has a clear declining trend with little spread in the data. However, this trend is indistinguishable from the climatological decline. In the week prior to the start of the storms, the average wind is close to zero with a large spread of values for the nine storms analyzed. But, in the day or two approaching the start of the storm, the average winds become more northerly and stronger in magnitude. After the typical storm duration length, the wind values return close to zero with a large spread in values. The third panel then shows a steady decline in SST values relative to the initial SST value over the three weeks analyzed.

Overall, the two categories with primarily northward advection tend to work against the climatological decline of ice. Table 3.2 summarizes the change in sea ice area for each of these four categories.

	ΔSIA (%)		
	3 days	1 week	2 weeks
Southward winds (-1.63 ms^{-1}) Increasing SST (0.056 °C day^{-1})	-26.9 (-17.4)	-31.8 (-22.7)	-35.3 (-27.9)
Northward winds (0.284 ms^{-1}) Decreasing SST (-0.046 °C day^{-1})	0.66 (-13.2)	-16.4 (-15.0)	-8.07 (-22.6)
Southward winds (-1.87 ms^{-1}) Decreasing SST (-0.048 °C day^{-1})	-11.1 (-9.17)	-14.3 (-12.0)	-15.9 (-12.1)
Northward winds (0.560 ms^{-1}) Increasing SST (0.059 °C day^{-1})	-2.15 (-17.5)	-6.97 (-24.8)	-24.6 (-32.6)

TABLE 3.2: Average change in sea ice area (SIA) for three days, one week, and two weeks after the storm start, relative to one week before the storm. Average climatological change is shown in parentheses. Each row also displays the mean meridional wind and mean SST changes across all storms in that category.

Chapter 4

Summary

4.1 Conclusions and Discussion

NSIDC sea ice observations, NOAA SST observations, and ERA5 reanalyses from 2007-2010 were examined to characterize the influence of Arctic cyclones on sea ice cover. Effects are found to vary depending on dominant wind direction and nearby SSTs. Two case studies reveal distinct mechanisms that may explain the wide-ranging sea ice responses to late-summer cyclones. In one case, northerly winds drive sea ice southward into warmer ocean waters. This advective process leads to gradual melt that has the potential to persist long after cyclone passage. Conversely, the second case analyzed had dominant southerly winds which drove sea ice northward into cooler ocean waters. This

second mechanism leads to a gradual increase in total sea ice area within the MIZ start-
ing a few days before the storm start and then continues to increase for the two weeks
analyzed after the storm.

The first case study analyzed lost about 36% of the initial ice area within the MIZ. This
result is representative of the average impact of other storms that fall into this category.
Out of all four categories, this storm type had the largest negative impact on the sea ice,
with increasing ice loss over the three weeks analyzed.

Conversely, the second case study resulted in a net gain of 46,600 km^2 of ice within the
MIZ over the 3-day storm duration. However, a week after the storm, the sea ice area is
approximately back to its original value. The category containing this case is the only
one out of the four that leads to a mean increase in ice area near the end of the storm.
Additionally, there is much greater variability in this mechanism. The spread of area
changes could result in either area increases or decreases.

Together, these two mechanisms account for only one-third of the responses within the
August and September 2007-2010 storm census examined here. The remaining two-thirds
of cases comprise storms that have primarily northerly winds but result in a decrease in
SST within the MIZ or storms that have primarily southerly winds but result in an
increase in SST within the MIZ. The cases with southward advection and a cooling SST
trend result in a sea ice trend that matches well with climatology, whereas the storms
with mean northward advection and warming SST category tend to increase the ice area

relative to the climatological melt. These two categories have the potential to enhance melt but otherwise simply redistribute ice within the MIZ.

4.2 Future Work

Within this study, 21 total storms were analyzed and categorized into four separate groupings, where the smallest category contained only two storms. To improve the statistical significance of these results, this categorization scheme must be expanded to include storms from additional years. We will also compare the characteristics of these late-summer storms to the cyclones that occur earlier in the melt season (i.e., June and July) when ice is more extensive and thicker. Another component of this expansion will be to compare cyclones from more recent years to earlier years. This comparison is possible since the datasets used in this study extend back to the 1980s. We hypothesize that due to recent decreases in Arctic ice extent, early-summer ice responses during the modern era will have similar responses to late-summer responses during earlier years.

An additional factor in this analysis is storm location and differences in storm development. The location where the storm develops can have different effects on not only the strength of the storm but also how the sea ice responds. A component that was not addressed above is the orientation of the ice edge relative to the storm winds. The first case study had meridional winds that were near-perpendicular to the ice edge. This finding is not necessarily true for the entire extent of the second case. Further investigation of how storms approach the ice edge and impacts the ice is recommended.

Also, the analysis presented in this thesis focuses almost exclusively on the relationship between cyclone near-surface winds and the sea surface temperature within the MIZ. Future analysis plans to incorporate additional factors that play a role in cyclone-induced sea ice changes. One primary aspect for future research is expanding ocean impact beyond the sea surface including investigating wave heights, currents, and vertical temperature profiles. The effect of cyclone-induced upwelling and upward heat transport plays an important role in sea ice changes (Peng et al., 2021, Zhang et al., 2013).

Another avenue to investigate as a potential source of variability among different cases is the potential for "pre-conditioning." When storms occur in sequence, previous storms can set up the ice in such a way that either enhances or minimizes the effect of the storms that follow (Parkinson and Comiso, 2013, Screen et al., 2011).

Lastly, the exact role of clouds and precipitation must be further defined. In the cases examined, the dynamic and thermodynamic effects appear to dominate, but the radiative effects of clouds could have the potential to amplify or minimize these effects. By incorporating these additional aspects of cyclone characteristics as well as expanding the number of cases analyzed, a more exact sea ice response can be identified.

Bibliography

Aizawa, T., and H. Tanaka, 2016: Axisymmetric structure of the long lasting summer arctic cyclones. *Polar Science*, **10 (3)**, 192–198.

Bekryaev, R. V., I. V. Polyakov, and V. A. Alexeev, 2010: Role of polar amplification in long-term surface air temperature variations and modern arctic warming. *Journal of Climate*, **23 (14)**, 3888–3906.

Box, J. E., and Coauthors, 2019: Key indicators of arctic climate change: 1971–2017. *Environmental Research Letters*, **14 (4)**, 045 010.

Carmack, E., and Coauthors, 2015: Toward quantifying the increasing role of oceanic heat in sea ice loss in the new arctic. *Bulletin of the American Meteorological Society*, **96 (12)**, 2079–2105.

Clancy, R., C. M. Bitz, E. Blanchard-Wrigglesworth, M. C. McGraw, and S. M. Cavallo, 2022: A cyclone-centered perspective on the drivers of asymmetric patterns in the atmosphere and sea ice during arctic cyclones. *Journal of Climate*, **35 (1)**, 73–89.

Comiso, J. C., 2012: Large decadal decline of the arctic multiyear ice cover. *Journal of climate*, **25 (4)**, 1176–1193.

Comiso, J. C., D. J. Cavalieri, C. L. Parkinson, and P. Gloersen, 1997: Passive microwave algorithms for sea ice concentration: A comparison of two techniques. *Remote sensing of Environment*, **60 (3)**, 357–384.

Finocchio, P., and J. Doyle, 2021: Summer cyclones and their association with short-term sea ice variability in the pacific sector of the arctic. front. *Earth Sci*, **9**, 738 497.

Finocchio, P. M., J. D. Doyle, D. P. Stern, and M. G. Fearon, 2020: Short-term impacts of arctic summer cyclones on sea ice extent in the marginal ice zone. *Geophysical Research Letters*, **47 (13)**, e2020GL088 338.

Gandin, L. S., 1963: Objective analysis of meteorological field. *Gidrometeorologicheskoe Izdate'stvo*, **286**.

Graham, R. M., S. R. Hudson, and M. Maturilli, 2019: Improved performance of era5 in arctic gateway relative to four global atmospheric reanalyses. *Geophysical Research Letters*, **46 (11)**, 6138–6147.

Hersbach, H., and Coauthors, 2020: The era5 global reanalysis. *Quarterly Journal of the Royal Meteorological Society*, **146 (730)**, 1999–2049.

Holt, B., and S. Martin, 2001: The effect of a storm on the 1992 summer sea ice cover of the beaufort, chukchi, and east siberian seas. *Journal of Geophysical Research: Oceans*, **106 (C1)**, 1017–1032.

Kapsch, M.-L., R. G. Graversen, M. Tjernström, and R. Bintanja, 2016: The effect of downwelling longwave and shortwave radiation on arctic summer sea ice. *Journal of Climate*, **29 (3)**, 1143–1159.

Kay, J. E., T. L'Ecuyer, A. Gettelman, G. Stephens, and C. O'Dell, 2008: The contribution of cloud and radiation anomalies to the 2007 arctic sea ice extent minimum. *Geophysical Research Letters*, **35 (8)**.

Koyama, T., J. Stroeve, J. Cassano, and A. Crawford, 2017: Sea ice loss and arctic cyclone activity from 1979 to 2014. *Journal of Climate*, **30 (12)**, 4735–4754.

Kriegsmann, A., and B. Brümmer, 2014: Cyclone impact on sea ice in the central arctic ocean: a statistical study. *The Cryosphere*, **8 (1)**, 303–317.

Kwok, R., G. Spreen, and S. Pang, 2013: Arctic sea ice circulation and drift speed: Decadal trends and ocean currents. *Journal of Geophysical Research: Oceans*, **118 (5)**, 2408–2425.

Landrum, L., and M. M. Holland, 2020: Extremes become routine in an emerging new arctic. *Nature Climate Change*, **10 (12)**, 1108–1115.

Lindsay, R., and A. Schweiger, 2015: Arctic sea ice thickness loss determined using subsurface, aircraft, and satellite observations. *The Cryosphere*, **9 (1)**, 269–283.

Meier, W. N., F. Fetterer, M. Savoie, S. Mallory, R. Duerr, and J. Stroeve, 2017: Noaa/nsidc climate data record of passive microwave sea ice concentration, version 3. boulder, colorado usa. nsidc: National snow and ice data center. doi:https://doi.org/10.7265/N59P2ZTG.

Ogi, M., I. G. Rigor, M. G. McPhee, and J. M. Wallace, 2008: Summer retreat of arctic sea ice: Role of summer winds. *Geophysical Research Letters*, **35 (24)**.

Parkinson, C. L., and J. C. Comiso, 2013: On the 2012 record low arctic sea ice cover: Combined impact of preconditioning and an august storm. *Geophysical Research Letters*, **40 (7)**, 1356–1361.

Peng, G., W. N. Meier, D. J. Scott, and M. H. Savoie, 2013: A long-term and reproducible passive microwave sea ice concentration data record for climate studies and monitoring. *Earth System Science Data*, **5 (2)**, 311–318, doi:10.5194/essd-5-311-2013, URL https://essd.copernicus.org/articles/5/311/2013/.

Peng, L., X. Zhang, J.-H. Kim, K.-H. Cho, B.-M. Kim, Z. Wang, and H. Tang, 2021: Role of intense arctic storm in accelerating summer sea ice melt: An in situ observational study. *Geophysical Research Letters*, **48 (8)**, e2021GL092 714.

Perovich, D. K., J. A. Richter-Menge, K. F. Jones, and B. Light, 2008: Sunlight, water, and ice: Extreme arctic sea ice melt during the summer of 2007. *Geophysical Research Letters*, **35 (11)**.

Reynolds, R. W., N. A. Rayner, T. M. Smith, D. C. Stokes, and W. Wang, 2002: An improved in situ and satellite sst analysis for climate. *Journal of climate*, **15 (13)**, 1609–1625, nOAA_OI_SST_V2 data provided by the NOAA/OAR/ESRL PSL, Boulder, Colorado, USA, from their Web site at https://psl.noaa.gov/data/gridded/data.noaa.oisst.v2.html.

Schreiber, E. A., and M. C. Serreze, 2020: Impacts of synoptic-scale cyclones on arctic sea-ice concentration: a systematic analysis. *Annals of Glaciology*, **61 (82)**, 139–153.

Screen, J. A., and I. Simmonds, 2012: Declining summer snowfall in the arctic: Causes, impacts and feedbacks. *Climate dynamics*, **38 (11)**, 2243–2256.

Screen, J. A., I. Simmonds, and K. Keay, 2011: Dramatic interannual changes of perennial arctic sea ice linked to abnormal summer storm activity. *Journal of Geophysical Research: Atmospheres*, **116 (D15)**.

Serreze, M., A. Barrett, J. Stroeve, D. Kindig, and M. Holland, 2009: The emergence of surface-based arctic amplification. *The Cryosphere*, **3 (1)**, 11–19.

Serreze, M. C., and R. G. Barry, 2011: Processes and impacts of arctic amplification: A research synthesis. *Global and planetary change*, **77 (1-2)**, 85–96.

Simmonds, I., and K. Keay, 2009: Extraordinary september arctic sea ice reductions and their relationships with storm behavior over 1979–2008. *Geophysical Research Letters*, **36 (19)**.

Simmonds, I., and I. Rudeva, 2012: The great arctic cyclone of august 2012. *Geophysical Research Letters*, **39 (23)**.

Sledd, A., and T. S. L'Ecuyer, 2021a: A cloudier picture of ice-albedo feedback in cmip6 models. *Frontiers in Earth Science*, **9**, 1067.

Sledd, A., and T. L'Ecuyer, 2021b: Emerging trends in arctic solar absorption. *Geophysical Research Letters*, **48 (24)**, e2021GL095 813.

Spreen, G., R. Kwok, and D. Menemenlis, 2011: Trends in arctic sea ice drift and role of wind forcing: 1992–2009. *Geophysical Research Letters*, **38 (19)**.

Stern, D. P., J. D. Doyle, N. P. Barton, P. M. Finocchio, W. A. Komaromi, and E. J. Metzger, 2020: The impact of an intense cyclone on short-term sea ice loss in a fully coupled atmosphere-ocean-ice model. *Geophysical Research Letters*, **47 (4)**, e2019GL085 580.

Stroeve, J. C., M. C. Serreze, M. M. Holland, J. E. Kay, J. Malanik, and A. P. Barrett, 2012: The arctic's rapidly shrinking sea ice cover: a research synthesis. *Climatic change*, **110 (3)**, 1005–1027.

Strong, C., and I. G. Rigor, 2013: Arctic marginal ice zone trending wider in summer and narrower in winter. *Geophysical Research Letters*, **40 (18)**, 4864–4868.

Tanelli, S., S. L. Durden, E. Im, K. S. Pak, D. G. Reinke, P. Partain, J. M. Haynes, and R. T. Marchand, 2008: Cloudsat's cloud profiling radar after two years in orbit: Performance, calibration, and processing. *IEEE Transactions on Geoscience and Remote Sensing*, **46 (11)**, 3560–3573.

Tsamados, M., D. Feltham, A. Petty, D. Schroeder, and D. Flocco, 2015: Processes controlling surface, bottom and lateral melt of arctic sea ice in a state of the art sea ice model. *Philosophical Transactions of the Royal Society A: Mathematical, Physical and Engineering Sciences*, **373 (2052)**, 20140 167.

Van Tricht, K., and Coauthors, 2016: Clouds enhance greenland ice sheet meltwater runoff. *Nature communications*, **7 (1)**, 1–9.

Winker, D. M., W. H. Hunt, and M. J. McGill, 2007: Initial performance assessment of caliop. *Geophysical Research Letters*, **34 (19)**.

Zhang, J., R. Lindsay, A. Schweiger, and M. Steele, 2013: The impact of an intense summer cyclone on 2012 arctic sea ice retreat. *Geophysical Research Letters*, **40 (4)**, 720–726.